Master Thesis

Julia Ribbrock

Modeling and flow control for a left ventricular assist device

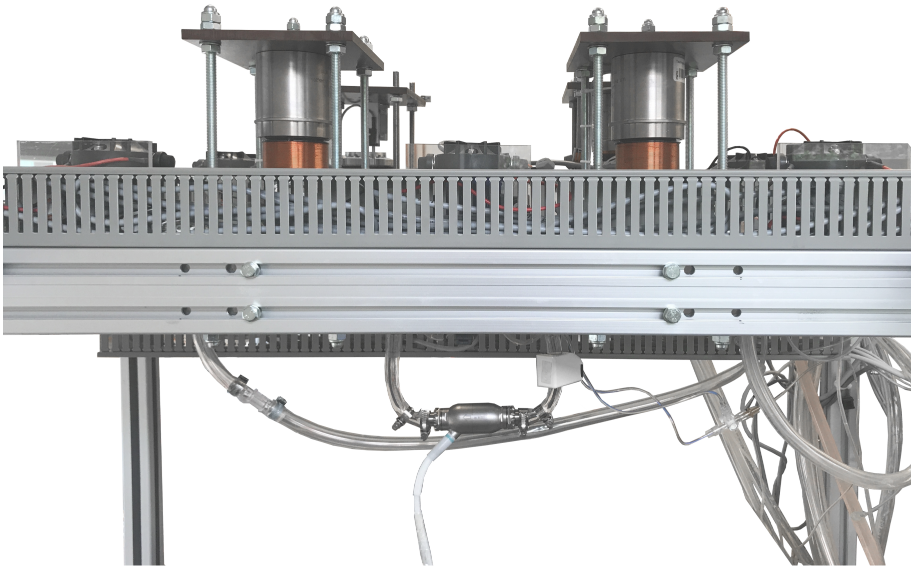

CHAIR FOR MEDICAL INFORMATION TECHNOLOGY

Faculty of Electrical Engineering and Information Technology, RWTH Aachen

Univ.-Prof. Dr.-Ing. Dr. med. Dr. h.c. Steffen Leonhardt

Supervisor: Patrick Borchers, M.Sc.

Date: January 5, 2021

Eidesstattliche Versicherung

Ribbrock, Julia
____
Name, Vorname

318927
____
Matrikelnummer (freiwillige Angabe)

Ich versichere hiermit an Eides Statt, dass ich die vorliegende Arbeit/Bachelorarbeit/ Masterarbeit* mit dem Titel

Modeling and flow control for a left ventricular assist device

selbständig und ohne unzulässige fremde Hilfe erbracht habe. Ich habe keine anderen als die angegebenen Quellen und Hilfsmittel benutzt. Für den Fall, dass die Arbeit zusätzlich auf einem Datenträger eingereicht wird, erkläre ich, dass die schriftliche und die elektronische Form vollständig übereinstimmen. Die Arbeit hat in gleicher oder ähnlicher Form noch keiner Prüfungsbehörde vorgelegen.

Aachen, 05.01.2021
____
Ort, Datum

____
Unterschrift

*Nichtzutreffendes bitte streichen

Belehrung:

§ 156 StGB: Falsche Versicherung an Eides Statt

Wer vor einer zur Abnahme einer Versicherung an Eides Statt zuständigen Behörde eine solche Versicherung falsch abgibt oder unter Berufung auf eine solche Versicherung falsch aussagt, wird mit Freiheitsstrafe bis zu drei Jahren oder mit Geldstrafe bestraft.

§ 161 StGB: Fahrlässiger Falscheid; fahrlässige falsche Versicherung an Eides Statt

(1) Wenn eine der in den §§ 154 bis 156 bezeichneten Handlungen aus Fahrlässigkeit begangen worden ist, so tritt Freiheitsstrafe bis zu einem Jahr oder Geldstrafe ein.

(2) Straflosigkeit tritt ein, wenn der Täter die falsche Angabe rechtzeitig berichtigt. Die Vorschriften des § 158 Abs. 2 und 3 gelten entsprechend.

Die vorstehende Belehrung habe ich zur Kenntnis genommen:

Aachen, 05.01.2021
____
Ort, Datum

____
Unterschrift

Abstract

Acute heart failure is one of the most common reasons for hospitalization due to heart disease. Because end-stage heart failure patients are dependent on a suitable donor heart and the number of cases far exceeds the number of available donor organs, acute heart failure often leads to patient death. Left ventricular assist devices (LVADs) have become a common treatment option for patients with heart failure when drug treatment is no longer sufficient. They assist the patient's heart in its function of pumping blood through the circulatory system and can thus prolong the time for adequate treatment with a donor heart.

The Sputnik VAD is an axial flow pump for left ventricular assistance, recently developed in Russia. Within the scope of this work, a system identification will be performed and different approaches for flow control will be implemented. For the controller implementation, PI controllers are designed according to different methods. Furthermore, the control loop is extended by including various iterative learning controllers. Initially, the goal is to enable regulating the flow to a constant reference. Eventually, however, reference tracking of a variety of reference trajectories is to be enabled. All controller implementations will be tested on a cardiovascular simulator developed at MedIT and their performance will be evaluated afterwards.

For the implementation of the ILCs, the approach of a parallel architecture with a PI controller is chosen. First, a standard ILC is designed and optimized under optimal, disturbance-free conditions. Based on this ILC, a disturbance in the form of the beating heart, simulated using the cardiovascular system simulator, is included in the control loop. A consideration of the ILC's ability to suppress non-repetitive disturbances revealed potential for improvement. Therefore, an attempt to optimize this capability was implemented in the form of a resampling functionality integrated into the ILC. The evaluation of the measurements showed an increased controller performance.

Contents

List of Figures

List of Tables

List of Symbols

Abbreviations

A	
AV	Atrioventricular
B	
bpm	beats per minute
BTD	Bridging to decision
BTR	Bridging to recovery
BTT	Bridging to transplantation
BVAD	Biventricular Assist Device
C	
CHR	Chien Hrones Reswick
CO	Cardiac Output
CVDs	Cardiovascular Diseases
CVS	Cardiovascular System
D	
DT	Destination therapy
E	
EDV	End-diastolic volume
EF	Ejection fraction
ESV	End-systolic volume
H	
HiL	Hardware in the Loop
HR	Heart rate
HTx	Heart transplantation

I

ILC	Iterative learning control
IMACS	International Mechanically Assisted Circulatory Support
INTERMACS	Interagency Registry for Mechanically Assisted Circulatory Support

L

LVAD	Left Ventricular Assist Device

M

MCL	Mock circulatory loop
MCS	Mechanical Circulatory Support
MISO	Multiple-input-single-output

R

RMSE	Root Mean Square Error
RWTH	Rheinisch-Westfälische Technische Hochschule

S

SISO	Single-input-single-output
SL	Semilunar
SV	Stroke Volume

V

VADs	Ventricular Assist Devices

W

WHO	World Health Organization

Z

ZN	Ziegler Nichols

1 Introduction

1.1 Motivation and goal

Heart failure is considered one of the most common cardiovascular diseases. The standard therapy for this disease is characterized by drug therapy and, last but not least, the implantation of a donor organ. However, since the number of patients who are dependent on a donor heart exceeds the number of available donor organs by far, which results in death of about 25 % of the patients waiting for a donor organ, it is necessary to develop new and improve already existing alternative forms of therapy [Sch10]. In case drug therapy is not sufficient to keep the patient alive until a heart transplantation can be performed, mechanical heart support systems of various kinds are increasingly used. Depending on the device used, the heart function can either be completely taken over by the device as would be the case with total artificial hearts, or a relief of the heart can be achieved by support via a ventricular assist device.
Within this work, the axial flow pump Sputnik VAD, which was developed in Russia, is used. This is an implantable left ventricular assist device providing continuous flow support used in bridging therapy until transplantation. As until now studies are not clear on whether a continuous flow profile introduces physiological difficulties for the patient, the aim of this work is to implement a flow control for the Sputnik VAD using Matlab and Simulink, which allows to adjust the flow to different predefined flow trajectories, continuous as well as pulsatile, by means of the continuous support system [MS09]. This goal will be achieved by implementing and evaluating different control algorithms. The testing of which will be performed using a cardiovascular system simulator developed at MedIT.

1.2 Thesis structure

This thesis aims to initially provide the reader with the necessary fundamental knowledge on the human cardiovascular system as well as basic information on the clinical syndrome of heart failure. Chapter 2 of this thesis, furthermore, provides an introduction to the therapeutic objective and the technology of ventricular assist devices. Following this, the basics of control engineering are explained in chapter 3. In particular, the structure and notation of a standard control loop, the operation and design of PI controllers, as well as the functionality and implementation of iterative learning controls are discussed.

Chapter 4 provides information on the Sputnik VAD and the circulatory system simulator of the Chair for Medical Information Technology. Furthermore, a system identification is performed through the acquisition of static maps for different test fluids and connection tube lengths.

The main part of this work is represented by chapter 5. This chapter deals with the implementation and evaluation of various control algorithms. At first two PI controllers are tuned, implemented and evaluated. Performance of these two controllers is compared in order to determine which controller provides the higher performance. The higher performing PI controller is then used as a stabilizing controller for an iterative learning control (ILC) implementation in form of a parallel architecture. Initially, various tests are performed to design the Q filter of the ILC. After successfully defining a cut off frequency for the filter, it is tested by using different reference flow trajectories. Initially, these tests are performed for repetitive disturbances, which are represented as a heartbeat of constant frequency using the test rig. Then, the ability of the ILC to also suppress non-repetitive disturbances in the form of variable heart rates is tested. These tests are of relevance for a later use of the system on the patient, since a constant heart rate cannot be guaranteed for the patient. In order to increase the performance of the ILC for this kind of disturbances, the standard ILC will finally be extended by a function which allows for resampling of the data to the iteration length corresponding to the current heart rate. For this implementation, tests are performed using different reference trajectories and the results are compared.

Finally, chapter 6 presents a summary of the findings of this thesis and offers an outlook on possible extensions of this thesis.

2 Medical Fundamentals

An important prerequisite to the work addressed in this thesis is comprehending the physiology of the cardiovascular system including the heart. Therefore, the theoretical foundations of this topic will be introduced in the following chapter.

2.1 Cardiovascular System

The fundamental task of the cardiovascular system is to supply all organs with blood through circulation. The human cardiovascular system is divided into two components, the systemic and the pulmonary circulation. The systemic circulation is supplying blood flow to all tissues and organs apart from the lungs. Figure 2.1 represents the blood distribution over the circulatory system. [Hal16]

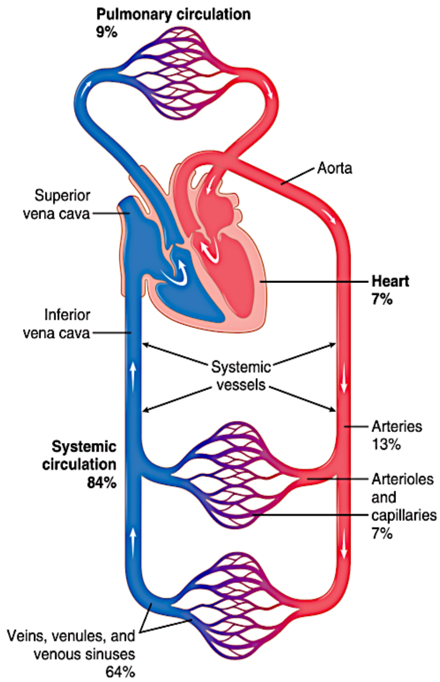

Figure 2.1: Blood distribution in the circulatory system [Hal16]. Red highlighting representing oxygenated, blue highlighting depicting deoxygenated blood flow.

The heart is the center of the cardiovascular system. It consists of two mechanical pumps, which are functionally connected in series but are united in one organ. It is separated into two sides, which themselves are divided into an atrium and a ventricle each. The atria act as weak primer pumps required to provide blood flow to the ventricles. [SLH11] Both the atria and the ventricles are surrounded by the myocardium, which serves as the working muscle of the heart. Through contraction of the myocardium, blood is pumped into the circulatory system. [SK07] The left ventricle is pumping oxygenated blood through the aorta into the systemic circulation. There, oxygen stored in the blood is delivered to the organs. The blood, now low in oxygen, is led into the right atrium through the inferior and superior vena cava. From the right atrium, the deoxygenated blood then enters the right ventricle. Afterwards, it is directed into the pulmonary circulation via the pulmonary artery. When the blood is oxygenated in the lungs, it is returned to the left atrium through the pulmonary vein. [SLH11] In addition to the atria and the ventricles, each side of the heart has an atrioventricular (AV) valve, as well as a semilunar (SL) valve. The AV valve of the left heart is called the mitral valve, the one of the right heart is referred to as the tricuspid valve. The aortic valve and pulmonary valve are the SL valves of the left and right heart, respectively. The valves determine direction of blood flow and thus prevent backflow. [SK07] A graphic overview of the anatomy and the course of blood flow through the heart is provided by Figure 2.2.

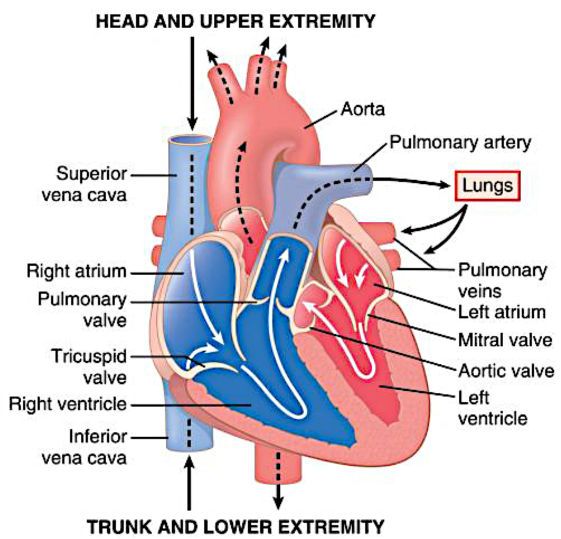

Figure 2.2: Anatomy of the human heart [Hal16]. Red highlighting representing oxygenated, blue highlighting depicting deoxygenated blood flow.

The amount of blood pumped through each side of the heart, called cardiac output (CO), is equal at all times. It is determined by multiplying the heart rate (HR) by the stroke volume (SV). For an average adult at rest with a heart rate of approximately $70\,min^{-1}$ and a stroke volume of $70\,ml$, this leads to

$$CO = HR \cdot SV = 70\,min^{-1} \cdot 70\,ml = 5\,l/min. \tag{2.1}$$

In case of maximum physical load, given at a stroke volume of $110\,ml$ and a heart rate of $190\,min^{-1}$, the cardiac output can increase to up to $20\,l/min$. [SLH11]
The cardiac cycle comprises all events that occur during the time-span of one heartbeat. The cycle is triggered by an electrochemical action potential originating from the sinus node. The cycle is divided into four phases. Figure 2.3 illustrates these action phases and events of the cardiac cycle for the left ventricle.

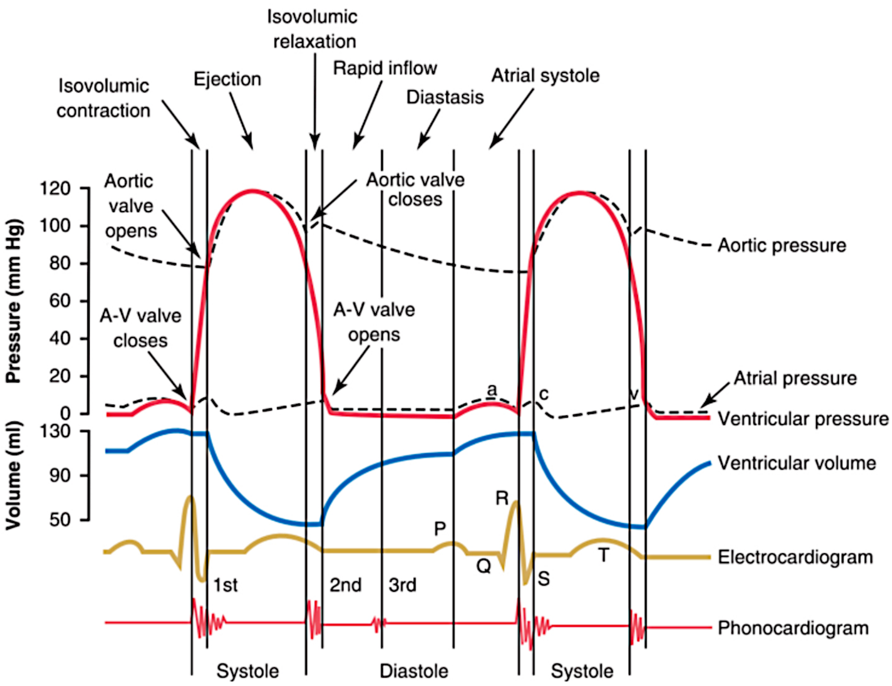

Figure 2.3: Action phases of the cardiac cycle based on the example of the left ventricle [Hal16].

During the period of isovolumic contraction, the ventricular pressure increases. For the left ventricle, the pressure increases from about $4-6\,mmHg$ to $80\,mmHg$, whilst the pressure values for the right ventricle are much lower. This increase is occuring as a direct result of the ventricular contraction. The AV valves, as well as the SL valves, are closed during this process, leading to a constant blood volume in the ventricles. As soon as the ventricular pressure exceeds the arterial pressure, the pulmonary and aortic valves open and blood can flow into the aorta and the pulmonary artery. This phase is called ejection phase, as blood is ejected into the circulatory system. The period of isovolumic contraction combined with the ejection phase comprises the ventricular systole. [SLH11] During systole, blood volume in the ventricle decreases by $55 - 60\,\%$, resulting in an end-systolic volume (ESV) of about $40 - 50\,ml$ [Hal16]. Due to the contraction of the myocardium, the ventricular pressure keeps increasing for a while before decreasing again as relaxation of the myocardium sets in. As soon as the outflow of blood ends, the semilunar valves close, initiating the period of isovolumic relaxation. During this period, pressure in the ventricles is decreasing while blood volume remains constant. When the pressure in the atrium exceeds the ventricular pressure, the AV valves open. This leads to blood flowing into the ventricles until pressure levels in the atria and ventricles are equalized. [SLH11] This phase is referred to as period of rapid filling of the ventricles. This period, in combination with the isovolumic relaxation, forms the diastole. The end-diastolic volume (EDV) amounts to about $110 - 120\,ml$. [Hal16] While at rest, the diastole lasts about twice as long as the systole. Above a heart rate of $150\,min^{-1}$ however, the two phases are about equal. [SLH11]

The pumping mechanism of the left ventricle can be illustrated using a pressure-volume diagram (P-V diagram). Construction of the P-V diagram first requires discussing the relationship between left ventricular volume and ventricular pressure during diastole and systole, as displayed in Figure 2.4a. The figure displays two curves named *diastolic pressure* and *systolic pressure*. Diastolic pressure is defined as the lowest point of each pulse during the relaxed state of the heart, whilst systolic pressure represents the highest point of each pulse, occurring while the heart is contracting and ejecting blood. [SLH11] The blue curve in Figure 2.4a, representing the diastolic pressure, is determined by gradually filling the heart with higher blood volumes and subsequently measuring the diastolic pressure just before ventricular contraction occurs. It describes the heart's mechanical properties when the myocardium is in a relaxed state. The green curve in Figure 2.4a, named systolic pressure, is plotted by measuring the systolic pressure over varying filling volumes for constant ventricle volumes. The red lines in Figure 2.4a and Figure 2.4b indicate the cardiac cycle and its four action phases, as described above. The line between points A and B in Figure 2.4b depicts the period of rapid filling.

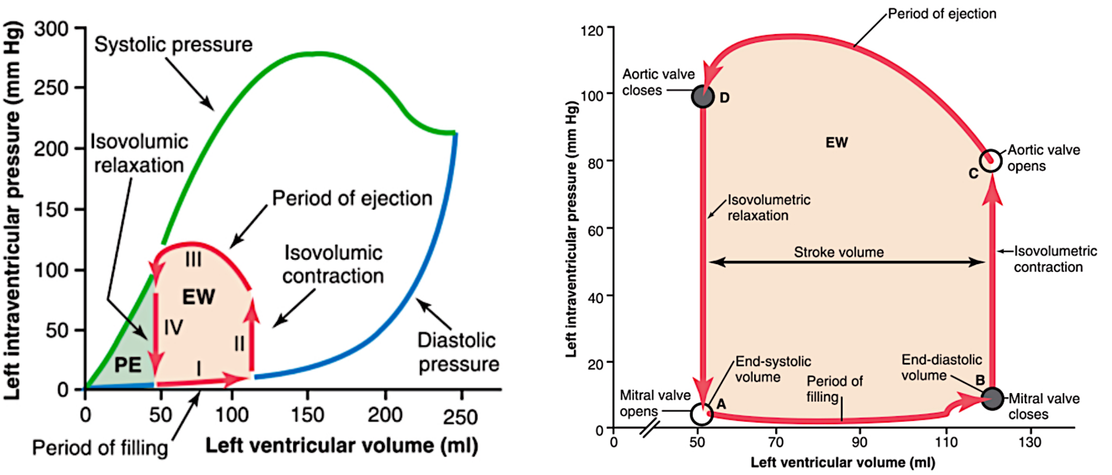

(a) **(b)**

Figure 2.4: (a) Working diagram of the left ventricle with P-V diagram. (b) Close-up P-V diagram. [Hal16]

The isovolumic contraction is represented by line II in Figure 2.4a, respectively between points B and C in Figure 2.4b. The ejection phase is depicted by III in Figure 2.4a and the line referred to as IV represents the period of isovolumic relaxation. The area of the work diagram, marked with EW in Figure 2.4 is a measure of the work done by the heart. The P-V diagram furthermore enables calculation of the ejection fraction (EF), which describes the percentage value of the ventricle volume ejected during systole. It is determined by

$$EF = \frac{SV}{EDV} \cdot 100. \tag{2.2}$$

For a healthy heart at rest, with a stroke volume of about $70\,ml$ and an EDV of about $100 - 120\,ml$, the EF amounts to about $50 - 60\,\%$. In cases of heart failure, the EF can decrease to about $20 - 25\,\%$. Therefore, knowledge of the P-V diagram is an important prerequisite in understanding myocardial diseases. [SLH11]

2.2 Heart failure

The World Health Organization (WHO) lists cardiovascular diseases (CVDs) as the global number one cause of death. In 2016, about 17.9 million people died from CVDs, representing 31 % of all global death that year. [Wor20]
In case of heart failure, the heart is unable to provide the required amount of blood flow to the cardiovascular system in order to supply all organs and tissue with oxygen. Heart failure does not directly represent a disease but rather a clinical syndrome. Nevertheless, the symptoms of different forms of heart failure are very similar and eventually manifest themselves in a decreased cardiac output. One acute consequence of heart failure, for example, is perceiving shortness of breath. In the long term, however, severe heart failure can also lead to muscle weakness and a lack of concentration.
According to Schmidt et al. [SLH11], heart failure can be attributed to either systolic or diastolic dysfunction. Systolic dysfunction can manifest itself in several ways. One is a reduced contractility and stroke volume of the heart. Causes may be, for example, a coronary artery disease that limits oxygen supply or a preceding myocardial infarction. Secondly, there may be increased pumping resistance due to an outflow obstruction. This may be the result of arterial hypertension, among other things. Furthermore, cardiac arrhythmias or a heart attack can lead to systolic dysfunction. Figure 2.5a displays the variation of the P-V diagram, comparing a normal functioning heart (dotted line) to one impaired by heart failure with a systolic dysfunction (solid line). In diastolic functional impairment, the dysfunction is evident in the course of the filling phase. This can be triggered, among other things, by reduced compliance of the myocardium due to hypertrophy or fibrosis. The change in the P-V diagram for diastolic heart failure is illustrated in Figure 2.5b. For treatment of heart failure, drug therapy using beta-blockers is initially targeted in most cases. However, if this is not successful, the use of ventricular assist devices can be a useful alternative in order to relieve the heart and provide sufficient blood flow. [SLH11]

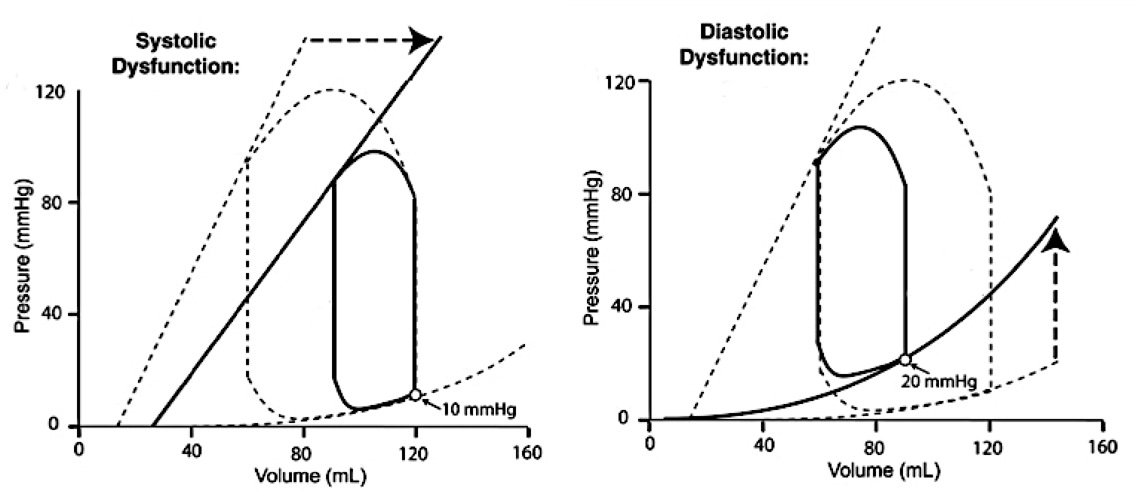

(a) (b)

Figure 2.5: P-V diagram for heart failure in case of (a) a systolic dysfunction and (b) a diastolic dysfunction according to [KR15]. The dotted lines symbolize normal heart function in comparison to the dysfunction represented by solid lines.

2.3 Ventricular Assist Devices

Despite heart transplantation (HTx) still being the gold standard for treatment of patients with terminal heart failure [Sch10], ventricular assist devices (VADs), as a kind of mechanical circulatory support (MCS) technology, are becoming increasingly important in treating patients with CVDs. There are two reasons for this. On the one hand, CVDs are gaining in importance due to demographic change. On the other hand, there is an increasing shortage of donor organs. [DMH19]

2.3.1 Therapeutic objective

Traditionally, the therapeutic goals of VAD treatment can be divided into three categories: *bridging to transplantation* (BTT), *bridging to recovery* (BTR) and *destination therapy* (DT). However in some cases, the classification into *bridging to decision* (BTD) and *bridging to transplantability* are mentioned additionally. The decision for

one of these goals is based on the type of CVD and the condition the patient is in when receiving VAD assistance. [KSS+11]
In clinical practice, different classification techniques connecting the patient's condition with the estimated survival time and the need for VAD assistance are used. An overview of the relation between the Interagency Registry for Mechanically Assisted Circulatory Support (INTERMACS) Score, the New York Heart Association(NYHA)-classification and the patient's condition is presented in Table 2.1.

INTERMACS Score	NYHA	Patient condition	Survival time
1	IV	critical cardiogenic shock	hours
2	IV	increasing catecholamine demand	days
3	IV	stable under inotropics	a week
4	IV	frequent decompensation	weeks-month
5	IV	rest discomfort/ not resilient	weeks-month
6	IV	rest discomfort/ merely resilient	month
7	IIIb	merely resilient	one year survival rate: 50-70%

Table 2.1: Relation between INTERMACS Score, NYHA-classification, patient condition and approximate survival time based on [Eif18].

The INTERMACS Score, which is based on data from patients which have received VAD treatment, links the need for a VAD to the appropriate time frame in which the device needs to be implanted. It is of high importance in deciding the therapeutic objective for VAD treatment. [DMH19]
The goal of *bridging to transplantation* is of great relevance with patients in NYHA-IV stadium showing hemodynamical instability. Due to a heart transplantation being the desired final treatment for these patients, there must be no contraindication to HTx. In case the patient does show a contraindication such as malignant tumors or an uncontrollable sepsis, the therapeutic objective changes from BTT to DT. In order for a treatment with a VAD as destination therapy being indicated, all conservative treatment options need to be exhausted. Due to the ever-growing shortage of donor organs, DT as a therapeutic approach in patients with heart insufficiency will become more relevant in the future even in cases usually suited for heart transplantation. [DMH19] There may occur some cases first contraindicating HTx, for

which the contraindication later on may dissolve. These indicate a therapy based on a *bridging to transplantability* goal. [KSS+11]
The indication for a *bridging to recovery* approach is twofold. Either the patient shows heart failure as a result of ischemia reperfusion damage or due to infectious genesis. In the first case the myocardium usually is able to recover within a few days, whereas in the second one the potential and the time necessary for recovery depend on how badly the tissue is damaged. In either scenario, a weaning from the VAD is an essential part of therapy. [DMH19]
If a patient is admitted in cardiogenic shock and medical treatment is not sufficient, *bridging to decision* becomes a relevant form of therapy. By providing the patient with a VAD, a more accurate assessment of the patient's condition is possible. Based on this, the decision on further treatment can be analysed more thoroughly. [KSS+11]

2.3.2 Technology

Since the first artificial blood-pump has been implanted in 1963, technology of VADs has improved significantly [LHH+63].
The general aim of ventricular assist devices is to provide mechanical support in pumping blood through the human body with the heart remaining inside the patient's body. Despite there being several types of VADs, all of them are working according to the same principle. Blood is taken from the circulatory system through the pump's inlet and ejected at another location via the pump's outlet. [LW16]
VADs are differentiated by three criteria: localization of the device inside the human body, flow profile and implantation strategy.
Regarding localization of the assistance device, three different options exist. With around 93 % of all implemented devices, the most commonly used ones are left ventricular assist devices (LVADs). [DMH19] LVADs are connected to the left ventricle, from where they are pumping blood into the aorta [GSL+03]. The second localization option is placing the device as support for the right ventricle. These devices are therefore called right ventricular assist devices (RVADs). RVADs are positioned in a way that blood is taken from the right atrium and ejected into the pulmonary artery. [DMH19] In some cases, RVADs in combination with the aforementioned LVADs are

used to build a biventricular assist device (BVAD). This type of heart support is mainly used for more severe heart diseases with high risk of developing right heart failure. [SH19]
The flow profile, as the second criterion for VAD distinction, is represented by pulsatile and continuous flow devices. Assistance with pulsatile devices can either be implemented to support the heart in a counter pulsation approach, working synchronous to the heart cycle, or as an asynchronous support. The most commonly known type of pulsatile device is a pneumatically driven pump ventricle. [LW16] However, according to the INTERMACS, over 95 % of all implanted devices are continuous flow devices [KPK+17]. These, in their most commonly used form, are electrically driven rotational blood pumps. A technological difficulty with these devices is the high probability of blood damage due to small gaps and very high rotational speed. However, these devices enable a dynamic adaption to the patient's physiological needs by being able to quickly adjust parameters such as the motor current. The possibility to keep track of these signal characteristics furthermore makes it possible to detect malfunctions or misplacement of the pump. [LW16]
Implantation of the VADs can be performed in one of three ways: paracorporeal, intracorporeal or percutaneous [DMH19]. For VAD systems which follow a paracorporeal approach, only the in- and outflow cannulas are located inside the human body. The cannulas are connecting the pump located outside the body with the ventricle and the vessels. Due to the pump being placed outside of the patient's body, these systems provide the option for pediatric MCS. This is not possible for most other systems due to the device being too large to fit inside a child's body. [SBL19] One example for paracorporeal systems are the aforementioned pneumatically driven pump ventricles [LW16]. In contrast to the paracorporeal devices, where the pump itself as well as its control unit are situated outside the body, in percutaneous devices the pump is placed inside the body. The control unit, however, remains outside the patient's body and is connected to the pump via leads. The intracorporeal devices are fully implanted into the body. [SBL19]
As far as the other two criteria for VAD differentiation are concerned, all combinations of localization and flow control are possible [SBL19]. As an example of a percutaneous device, [DMH19] names the Impella 2.5, a rotary blood pump with continuous flow used for left ventricular assistance.

The proportions of different VAD types and therapeutic goals, as based on the International Mechanically Assisted Circulatory Support (IMACS) register are illustrated in Table 2.2.

VAD type		Therapeutic objective	
LVAD	93%	DT	40%
BVAD	4%	BTD	30%
TAH	2%	BTT	29%
unknown	0.1%	others (BTR, ...)	1%
RVAD	0.05%		

Table 2.2: Percentages of VAD types and therapeutic objectives in mechanical heart support based on [DMH19].

3 Control Theory

Since this thesis addresses the implementation of flow control algorithms for a left ventricular assist device, this section will focus on the fundamentals of notation and structure of a standard control loop. Furthermore, the basic principles of PI-controllers and iterative learning control (ILC) are discussed, since these are used within the practical part of the thesis.

3.1 Fundamentals

The basic task of control engineering is to externally influence a time-varying process with the goal of executing the process in a predetermined manner. A control system is characterized in particular by the feedback of the controlled variable to the reference variable. The reference variable comprises the state that has to be achieved. In theory, this is represented by a control loop with the components shown in Figure 3.1. The plant $G(s)$ transfers the actuating variable $u(t)$, as well as the influence of the the disturbance $d(t)$, to the controlled variable $y(t)$. This variable is permanently compared with the reference variable $w(t)$ by means of a feedback loop, providing the control error

$$e(t) = w(t) - y(t). \tag{3.1}$$

The controller $G_{\mathrm{c}}(s)$ then transforms the control error to the actuating variable again. The aim of the control loop is to achieve the smallest possible control error with the highest possible damping. Since these goals contradict each other, a trade off must

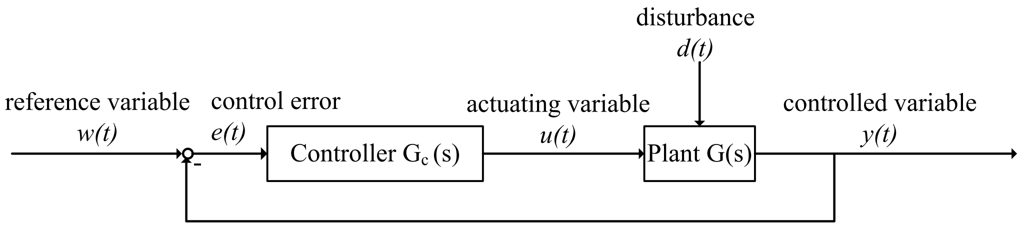

Figure 3.1: General structure of a control loop

always be accepted here. [ZR17]
However, there are some general requirements for the closed control loop which have to be fulfilled. The first requirement states that the closed loop needs to be stable, which is met if the control loop responds to a finite excitation with a finite output signal. The second condition is the requirement for disturbance rejection, stating that the controlled variable needs to follow the reference variable asymptotically, so that

$$\lim_{t \to \infty} e(t) = 0. \tag{3.2}$$

Another requirement is that the dynamic relationship between the reference variable $w(t)$ and the controlled variable $y(t)$ must satisfy specified quality requirements. Finally, these three requirements must be satisfied despite uncertainties in the plant, forming the robustness requirement. More detailed information on these requirements can be found in [Lun10].

The plant $G(s)$ corresponds to the part of the system in which the physical quantity to be controlled is influenced by the controller. The calculation of the plant by setting up and solving differential equations is possible only in a few cases. Furthermore, calculation in many cases is very time consuming. Due to this, the determination of the plant's characteristic values is usually carried out experimentally. There are several basic types of plants, classified according to their dynamic behavior. As only the PT_1-element is used in the practical part of this thesis, all other variations will not be discussed at this point. Detailed information on this topic can be found in [Lun10].
The PT_1-element is the plant type which is most common in technical equipment. A PT_n-element in its steady state reacts proportionally to the input value and has a distinct transition behavior. The index n describes the order of the system. Therefore, a PT_1-element is a proportional delay element of first order. The mathematical formulation of the transfer function of a PT_1-element is

$$G(s) = \frac{k_\mathrm{s}}{1 + sT}. \tag{3.3}$$

The value k_s describes the static gain, which for a unit step and $h(t = 0) = 0$ is defined as

$$k_\mathrm{s} = h(t \to \infty). \tag{3.4}$$

The time constant T gives an impression of the speed with which the system can react to changes at the input. It is defined as the time at which the transfer function reaches 63 % of its static gain. [Lun10] Figure 3.2 shows the transfer function of a PT_1-element (blue curve) and its significant parameters.

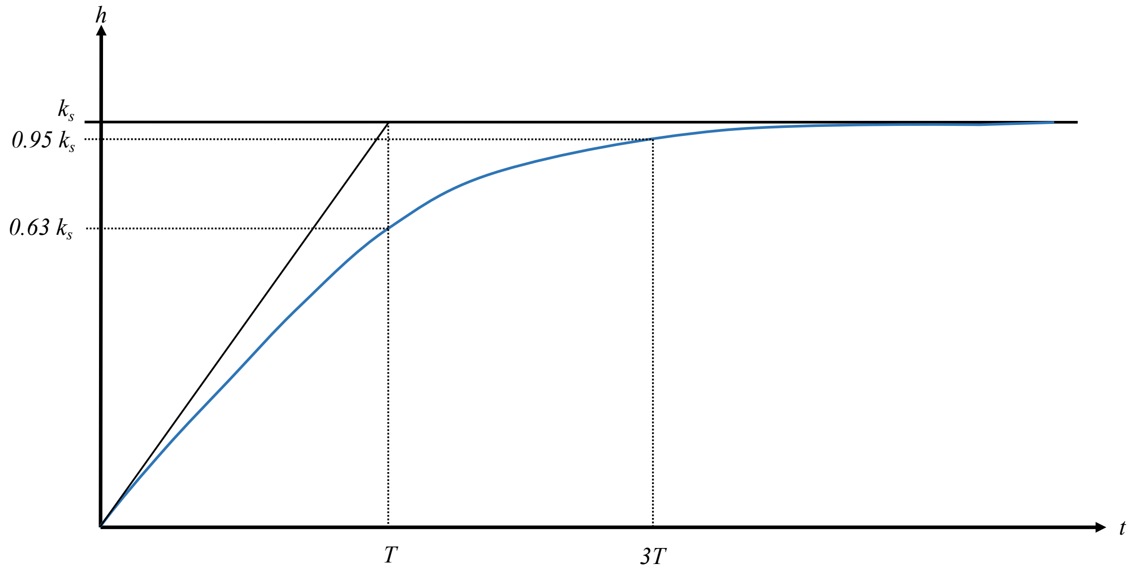

Figure 3.2: Transfer function of a PT_1-element [Lun10].

3.2 PI-controller

A PI-controller is a control structure commonly used for linear systems. This structure consists of both a proportional (P) and an integral (I) control element. The output value of a P-controller is proportional to its input value. In relation to the control loop in Figure 3.1 this leads to

$$u(t) = K_{\mathrm{P}} e(t). \tag{3.5}$$

Using Laplace transformation, the transfer function for a P-controller can be determined as

$$G(s) = \frac{u(s)}{e(s)} = K_{\mathrm{P}}. \tag{3.6}$$

Therefore, the step response of this controller equals a step weighted with the parameter K_{P}.
The relationship between input and output value of an I-controller is described through

$$u(t) = K_{\mathrm{I}} \cdot \int e(t)dt. \tag{3.7}$$

Just as for the P-controller, Laplace transformation can be used to determine the transfer function of the I-controller. This leads to

$$G(s) = \frac{u(s)}{e(s)} = \frac{K_{\mathrm{I}}}{s}, \tag{3.8}$$

which indicates a step response in form of a ramp with slope K_{I}. In order to generate a PI-controller, the elements from (3.5) and (3.7) can be added, which leads to

$$u(t) = K_{\mathrm{P}}e(t) + K_{\mathrm{I}} \cdot \int e(t)dt. \tag{3.9}$$

Laplace transformation can be used again to compute the transfer function

$$G(s) = \frac{u(s)}{e(s)} = K_{\mathrm{P}} + \frac{K_{\mathrm{I}}}{s}. \tag{3.10}$$

The step response of the PI-controller, illustrated in Figure 3.3, shows both the weighted step from the P-controller and the ramp from the I-controller.

3.2.1 Tuning rules

Tuning the controller parameters, i.e adjusting their values depending on the system, is of great importance. Incorrectly chosen parameters can lead to poor performance or unstable system behavior, which may result in system damage. There are many different approaches to tune a PI-Controller in order to achieve optimal system performance. These range from heuristic methods over analysis of pole-zero plots to computer-aided numerical parameter optimization. [Lun10] At this point, the tun-

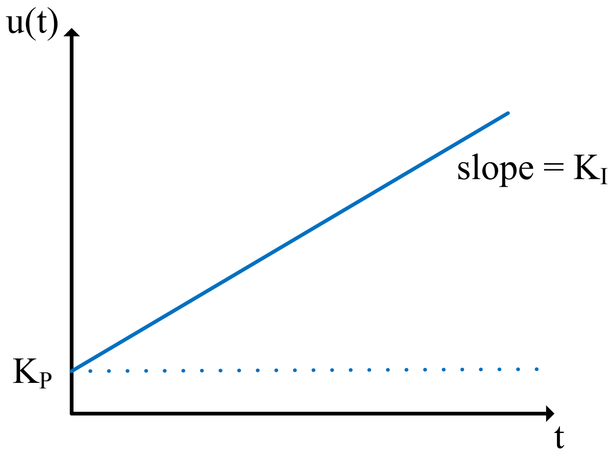

Figure 3.3: Step response of a PI-Controller based on [ZR17].

ing rules according to Ziegler Nichols (ZN) and the rules according to Chien Hrones Reswick (CHR) will be discussed, as these are used for the implementation of flow control in the practical work. Information on other approaches can be found in [AHR11].

Tuning rules according to Ziegler Nichols

The tuning rules according to Ziegler Nichols are one of the most commonly used heuristic methods in tuning controller parameters for PI-controllers. They are used especially if a mathematical model of the plant is not available but the plant can be approximated as a $\mathrm{PT_n}$-element. [ZR17] A necessary condition is the possibility to experimentally identify the step response of the plant without risk of damage to the system. After the step response has been determined, it is displayed graphically. Then the inflection tangent is drawn into the step response as shown in Figure 3.4. The blue line represents the step response, the red line the inflection tangent, respectively. The gain K_S, the delay time T_v and the settling time T_g can be read from the graph. Using these, following [ZR17], the factor K_P is calculated as

$$K_\mathrm{P} = 0.9 \cdot \frac{T_\mathrm{g}}{K_\mathrm{S} T_\mathrm{v}}. \tag{3.11}$$

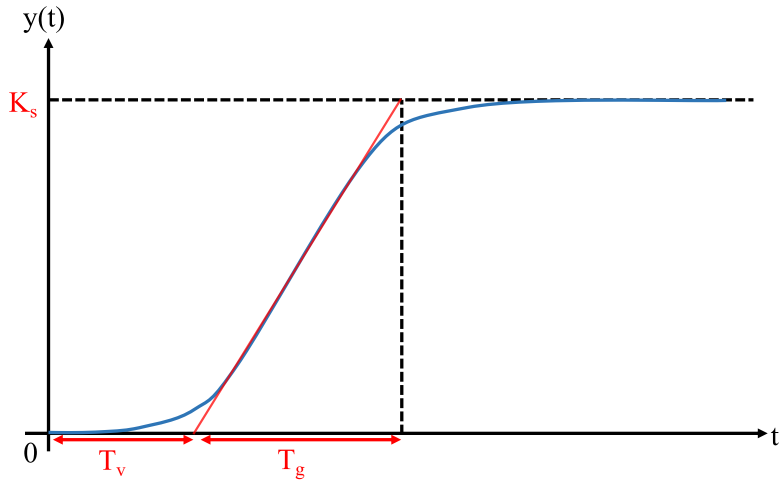

Figure 3.4: Inflection tangent method for Ziegler Nichols and Chien Hrones Reswick based on [ZR17].

The factor K_{I} is calculated according to:

$$K_{\mathrm{I}} = \frac{K_{\mathrm{P}}}{T_{\mathrm{N}}}, \tag{3.12}$$

with

$$T_{\mathrm{N}} = 3.3 \cdot T_{\mathrm{v}}. \tag{3.13}$$

Tuning rules according to Chien Hrones Reswick

The tuning method according to Chien Hrones Reswick is very similar to the one by Ziegler Nichols. However, this method provides the ability to adjust the transient response of the control loop. The tuning parameters can either be chosen in a way to provide an overdamped behavior or a course providing 20 % overshoot. [AHR11] For both options, the step response and its inflection tangent are graphically displayed, as for the Ziegler Nichols approach in Figure 3.4. The values for K_{S}, T_{v} and T_{g} can be read from the plot. The parameter value K_{I} again is calculated following (3.12). The formulas for calculating K_{P}, T_{N} and T_{D} are given in Table 3.1.

overdamped		20% overshoot	
K_{P}	T_{N}	K_{P}	T_{N}
$0.35 \cdot \frac{T_{\mathrm{g}}}{K_{\mathrm{S}} T_{\mathrm{v}}}$	$1.2 \cdot T_{\mathrm{v}}$	$0.6 \cdot \frac{T_{\mathrm{g}}}{K_{\mathrm{S}} T_{\mathrm{v}}}$	T_{v}

Table 3.1: Tuning parameters according to Chien Hrones Reswick based on [ZR17].

3.3 Iterative Learning Control

The use of iterative learning control aims to improve control performance for systems which execute the same task repeatedly under constant operating conditions. This improvement is based on the idea that it is possible to include error information from previous iterations into the adjustment of the actuation variable during the current iteration. The standard control structure of an ILC algorithm is presented in Figure 3.5.

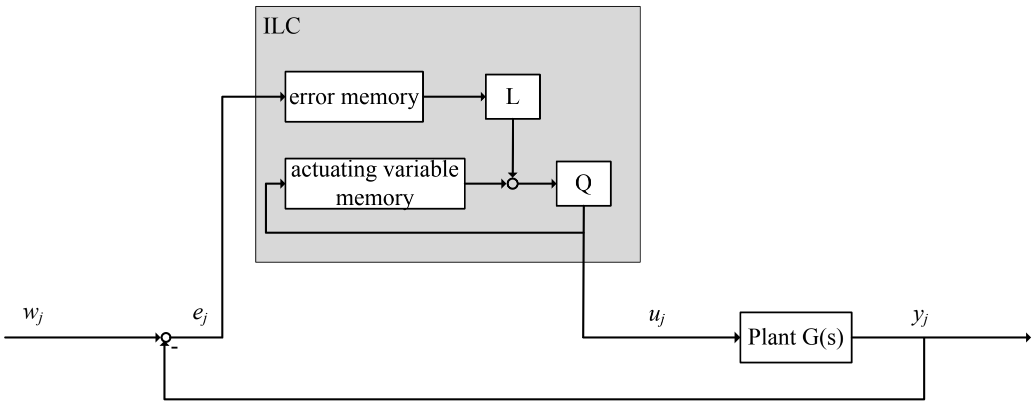

Figure 3.5: Standard ILC control loop based on [BTA06].

Considering a linear-time-invariant single-input-single-output (SISO) system, the ILC learning algorithm is as follows:

$$u_{\mathrm{j}+1} = Q(q)[u_{\mathrm{j}}(k) + L(q)e_{\mathrm{j}}(k+1)] \tag{3.14}$$

where k is the time index, j is the iteration index, q is the forward time-shift operator $qx(k) \equiv x(k+1)$, $Q(q)$ is defined as the Q-filter and $L(q)$ represents the learning function. The performance error signal e_{j} is defined as

$$e_{\mathrm{j}} = w_{\mathrm{j}} - y_{\mathrm{j}}. \tag{3.15}$$

Feedback controllers such as PI-controllers are only able to consider the current changes in control error. By taking into account the information from previous iterations, low tracking errors are achievable through an ILC. This results in exceptional performance with convergence during the first few iterations. This can be achieved even for systems prone to repeating disturbances and model uncertainties. While feedback control shows a lag in transient tracking due to reacting to inputs and disturbances, ILC, as a feedforward controller, does not. Another advantage of ILC use is that there is no need for disturbances to be known or measured, as long as these signals show repeating behavior during each iteration. Furthermore, by storing signal information during each iteration, ILC enables advanced filtering and signal processing of the control error. However, ILC utilization holds some issues in regard to non-repeating disturbances or noise influences. In these cases it may be useful to combine ILC approaches with a feeback controller. A combination of the systems is furthermore required if the behavior of the plant is not stable. [BTA06] A parallel architecture of a feedback controller in combination with an ILC is illustrated in Figure 3.6.

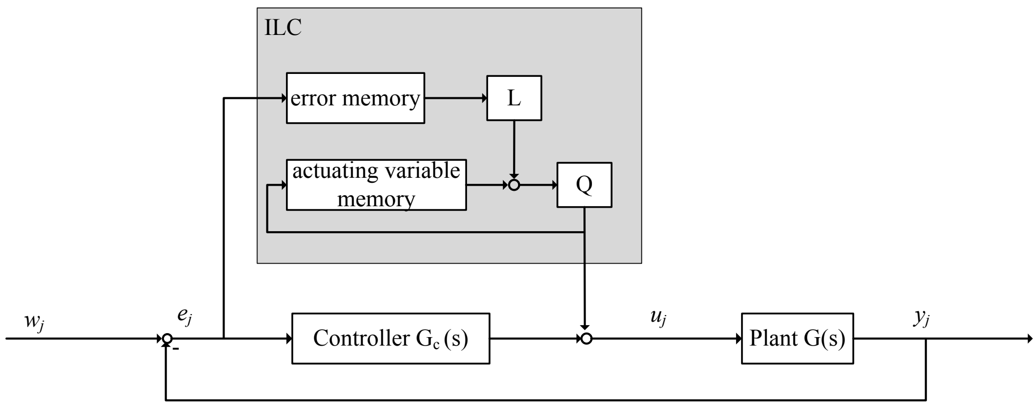

Figure 3.6: Parallel architecture of ILC with feedback controller based on [BTA06].

There are several approaches to design an ILC. In general, an ILC ideally learns only the repeating disturbance patterns without being influenced by noise. The most common types of ILC learning functions are the P-, D- and PD-type learning func-

tions. As an ILC does have a natural integrator action from one iteration to the next, I-type learning functions are rarely used.
The discrete-time learning function for a standard PD-type ILC is given as

$$u_{\mathrm{j+1}}(k) = u_{\mathrm{j}}(k) + k_{\mathrm{p}} e_{\mathrm{j}}(k) + k_{\mathrm{d}}[e_{\mathrm{j}}(k+1) - e_{\mathrm{j}}(k)]. \tag{3.16}$$

k_{p} represents the proportional gain while k_{d} is the derivative gain. In case a P-type learning function is implemented, the derivation gain is set to $k_{\mathrm{d}} = 0$. For a D-type learning function, $k_{\mathrm{p}} = 0$ is used, respectively.
The performance of these ILC types depends mainly on accurate parameter tuning and does not require an accurate mathematical model of the plant. Despite these approaches being frequently used, there are no tuning guidelines similar to the ones mentioned for PI-controller tuning. However, a commonly used way to influence the process behavior is to modify the learning algorithm to include a Q-filter. This filter can be used to disable learning at high frequencies in order to filter noise at these frequencies. This increases robustness of the system. First, a filter type such as Butterworth or Chebyshev is specified. The bandwidth can then be interpreted as a tuning parameter in addition to the proportional gain k_{p}. Initially, learning gain and filter bandwidth are set to low values. When a steady baseline behavior and error performance is achieved, the parameter values can be increased to improve performance. The learning gain influences the rate of error convergence while the Q-filter influences the error performance. Performance increases proportionally with filter bandwidth. However, this includes a trade-off with robustness. For lower filter bandwidth, high robustness can be achieved in a trade-off with performance.
Besides the P-,D- and PD-type ILC there are other design approaches. The H_∞ method can be used to design a robustly convergent ILC controller, with a trade-off in performance. A quickly converging ILC approach can be achieved by using the plant inversion method. This however depends on accurate modeling of the plant. The quadratically optimal ILC approach uses quadratic performance criteria to design an optimal ILC. Further information on these alternative design methods is provided in [BTA06].

4 Identification

4.1 Sputnik VAD

The Sputnik VAD is an axial-flow blood pump, developed in a cooperative project of the National Research University of Electronic Technology, OJSC Zelenograd Innovation-Technology Center of Medical Equipment, FSBI "Academician V.I. Shumakov Federal Research Center of Transplantology and Artificial Organs", Ministry of Health of Russian Federation, DONA-M LLC and BIOSOFT-M LLC in 2009. [ST15]
This device is used for left ventricular assistance in patients with acute heart failure. The therapeutic objective in implantation of a Sputnik VAD is bridging to transplantation. The VAD is able to pump up to 10 liters of blood per minute with a continuous flow profile. The implantable pump weighs about $200\,g$, has a length of $81\,mm$ and a maximum diameter of $34\,mm$. It consists of a moving and a stationary part. The moving part, the impeller, a rotor with four blades, contains a permanent NdFeB-magnet, which is actuated by a brushless DC motor. The rotor spins clockwise with speed values between $4000 - 10000\,rpm$. An overview of the pump's specification is presented in Table 4.1.

Blood flow	0-10 l/min
Rotational speed	4000-10000 rpm
Length	81 mm
Diameter	34 mm
Weight	200 g

Table 4.1: Specifications of Sputnik VAD

The stator is located inside a titanium housing with a diameter of $16\,mm$. The stationary part of the pump consists of a flow straightener with three stationary blades and a flow diffusor with three twisted blades. The flow straightener is located in front of the rotor and straightens the incoming blood flow into the rotor. Behind the rotor, blood is directed into the diffusor. Figure 4.1 depicts a cross-section of the Sputnik VAD and identifies its individual components. The connection between the pump and the cardiovascular system is realized by using in- and outflow cannulas, a felt ferule and vascular prosthesis which is sewed to the aorta. [ST15]

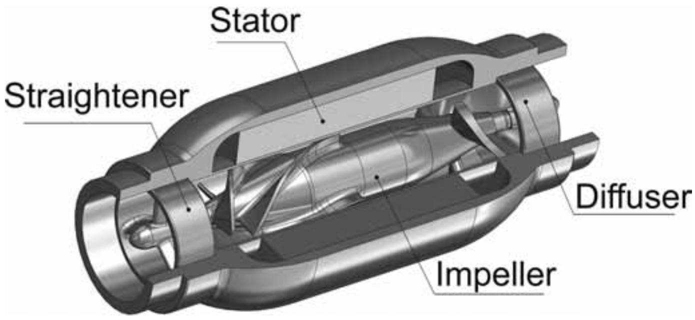

Figure 4.1: Cross-section of the Sputnik VAD [ST16].

The Sputnik VAD is powered using two lithium-ion batteries, fully charged providing enough energy for up to eight hours of system support. The maximum charging time for the batteries is less than five hours. During this time the batteries can either be exchanged by another set of batteries or the system can be powered through connection to an AC network. A microprocessor-based driving unit is used to regulate the pump speed, manage the power supply and store parameter data. It is connected percutaneously to the pump with an up to 170 cm long and 5 cm wide lead. [ST15] During the practical part of this work, the pump was controlled using the servo controller module ESCON 50/4 EC-S from maxon motor. This is a 4-quadrant pulse width modulation controller for controlling motors without Hall sensors.

4.2 Hardware in the Loop Test Bench

For all measurements and tests performed during this thesis, a hardware in the loop (HiL) test bench of the Chair of Medical Information Technology at RWTH Aachen University is used. The test bench is set up as a feedback controlled human circulatory system simulator. With the aid of the test rig it is possible to test MCS systems under various physiological and pathological conditions of the cardiovascular system.

The structure of the mock circulatory loop (MCL) is depicted in Figure 4.2. The boxes marked V_1 and V_2 are pressure compartments simulating the volume of the left

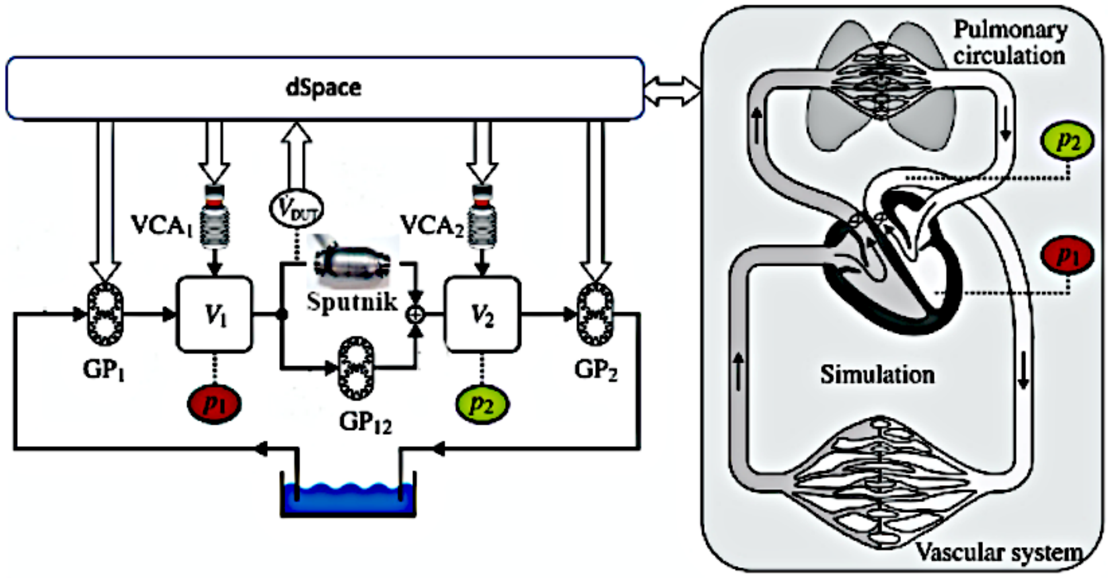

Figure 4.2: Structure of the HiL human circulatory system simulator based on [MRS+15]. Pressure chambers: V_1 and V_2, gear pumps: GP_1,$GP_{1,2}$ and GP_1, left ventricular pressure: p_1, pressure in aorta: p_1, flow measured by flowmeter: $\dot{V}_{\mathrm{DUT}}$.

ventricle and the aorta, respectively. Therefore, the pressure values of these compartments, referred to as p_1 and p_2, can be physiologically compared to the pressure values of the left ventricle and aorta. The MCL is actuated by three gear pumps (GP_1, GP_{12} and GP_2) and two voice coil actuators (VCA_1 and VCA_2). The Sputnik VAD is connected to the pressure chambers in parallel, enabling tests similar to real use cases. This way, the VAD can be subjected to comparable pressure changes in the differential pressure between the aorta and ventricle as would be the case when used on the beating heart.

By controlling the MCL through a dSpace system (DS1103), pressure in the chambers can be adjusted in real time to simulate different cardiac dysfunctions. The dSpace system furthermore enables recording of reference signals presented to the MCL, as well as real time measurements.

As the Sputnik VAD is not usually included into the MCL setup, flow through the device can not be measured without further equipment. For this purpose the Transonic Systems Inc. T110 flowmeter is included in the setup. The flow sensor measurement is based on ultrasonic technology. The sensor probe, as presented in Figure 4.3, is mounted onto the tube representing the connection between left ventricle and the VAD. The flowmeter too is connected to the dSpace system, enabling recording of the measured flow values. In Figure 4.2 the measurement of the device is represented by $\dot{V}_{\mathrm{DUT}}$.

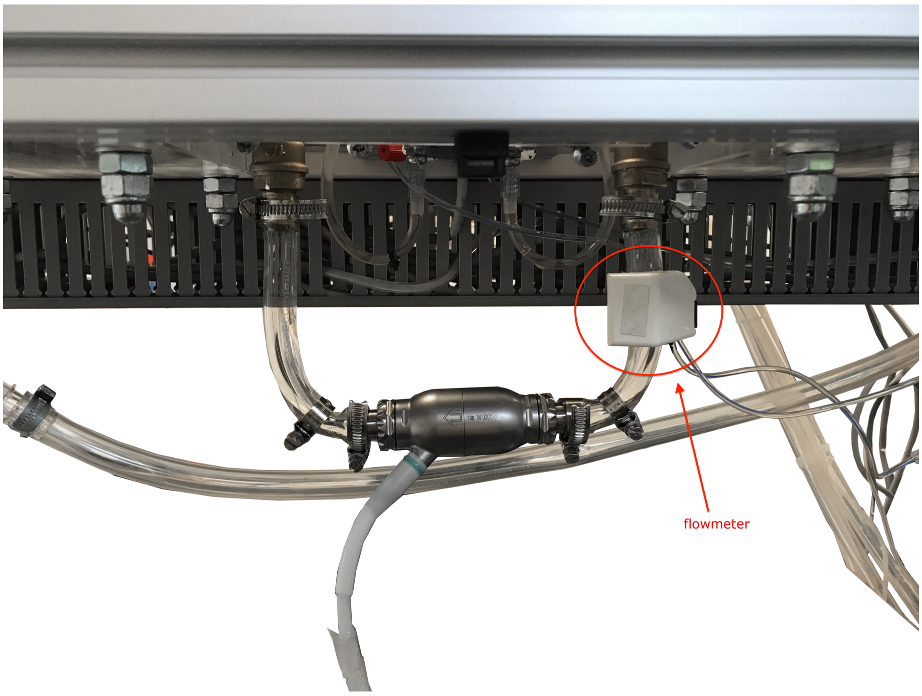

Figure 4.3: Sputnik VAD and flowmeter in HiL setup.

The ESCON servo controller mentioned in chapter 4.1, as well as the flowmeter and the MCL, is connected to the dSpace system. Using the digital input port of the controller, a set value for regulation of the rotational speed can be transferred to the controller after defining the value in the system.
The dSpace system itself is controlled with the use of the program ControlDesk. This software provides the opportunity to include Matlab and Simulink source code. By this, controllers designed with the use of Simulink can directly be tested at the HiL test bench. It furthermore enables exporting all measured data in form of Matlab matrices.

4.3 System Identification

For the implementation of flow control algorithms for the Sputnik VAD, knowledge of the system behavior is required. In order to gain this information, various tests are performed to determine a static map for the system. For this purpose, a multiple-input-single-output (MISO) system with input variables differential pressure Δp in $mmHg$, rotational speed v in rpm and output variable blood flow q in l/min is assumed. The differential pressure is defined as

$$\Delta p = p_{\text{ao}} - p_{\text{lv}} = p_2 - p_1, \tag{4.1}$$

with p_{ao} depicting the pressure of the aorta and p_{lv} corresponding to the left ventricular pressure.
Using the HiL test rig, the differential pressure is increased in steps of $20\,mmHg$ starting at $0\,mmHg$ and ending at $140\,mmHg$. For each differential pressure step, the reference speed of the pump is increased from $4000\,rpm$ in steps of $1000\,rpm$ to $9000\,rpm$. Flow for each reference speed is measured for $5\,s$. In order to eliminate inaccuracies due to transient processes, solely the last quarter of each mesurement stage is considered for the evaluation using Matlab. Figure 4.4 depicts the signal curves for the measurement described above. The upper graph shows the course of the reference differential pressure (Δp_{ref}) and the differential pressure measured at the HiL test stand (Δp_{HiL}). In the middle, the curves of the reference velocity (v_{ref}) and the measured velocity of the Sputnik VAD (v_{vad}) are shown. The lower graph shows the resulting flow through the blood pump (q_{vad}).

To determine the static map, flow data is first broken down into individual parts corresponding to the various differential pressure levels. These are then split into data sections for each velocity rate. Finally, the mean of the last quarter of each section is calculated. The average flow values are then displayed as a function of differential pressure. The values of equal velocity levels are connected with each other.
At the beginning of the practical work, the Sputnik VAD was connected to the test stand via tubes of about $30\,cm$ length on both sides. Since in clinical use, the pump is implemented in the patient's body and connected to the left ventricle and aorta, the tube length is not representative of a real application. To test the effect tube length has on the operating range of the pump, three different tube lengths for attachment

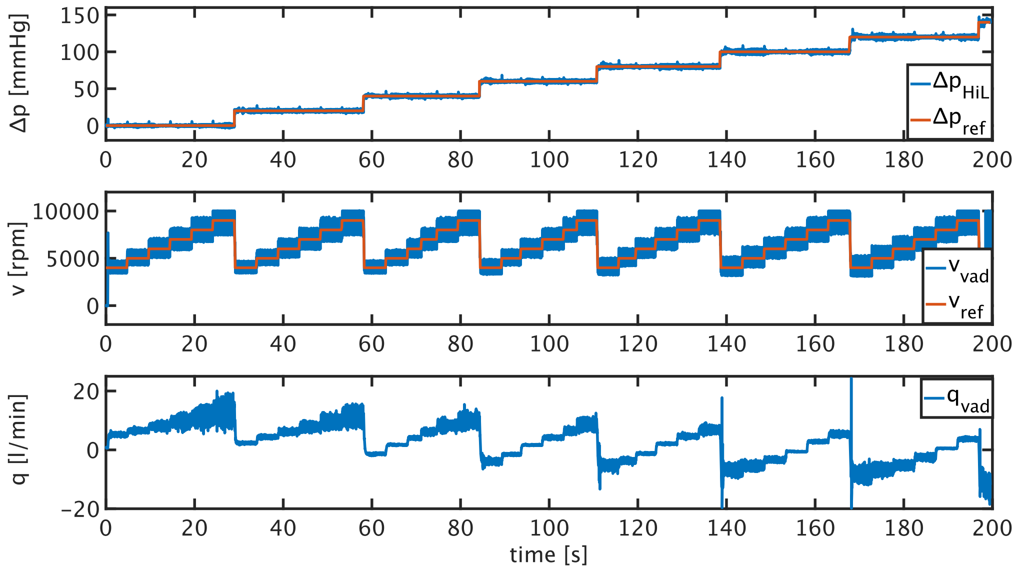

Figure 4.4: Signal curves for creation of the static map for 60 % water, 40 % glycerin solution with 15 cm long tubes. Top: differential pressure, middle: rotational speed, bottom: flow through VAD.

of the VAD to the test rig are compared. The measurements are performed with tubes of approximately 5 cm, 10 cm and 15 cm length. Figure 4.5 depicts the static maps for all three tube lengths measured with a fluid solution of 60 % water 40 % glycerin.

Under inspection of the blue curves corresponding to a tube length of 5 cm it is evident that measurements in this case were only performed up to a differential pressure of $\Delta p = 100\,mmHg$. This is a result of the abrupt change in differential pressure and reference speed which leads to spontaneous reduction of the flow and possibly high backflow values through the pump. As a result, the pump's rotor stops. For longer tubes (10 cm and 15 cm length) and therefore higher flow resistance, this phenomenon occurs at a differential pressure of $\Delta p = 140\,mmHg$. However, the deviation of the curves is insignificant when comparing all three cases. Due to this the tubes of 15 cm length were chosen for reasons of improved handling of the MCL.

In addition to different tube lengths, another preliminary investigation is carried out with regard to the influence of the test liquid used. Since blood viscosity varies between patients and also with fluid intake, knowledge on the effect a change in liquid condition has on the control performance is required.

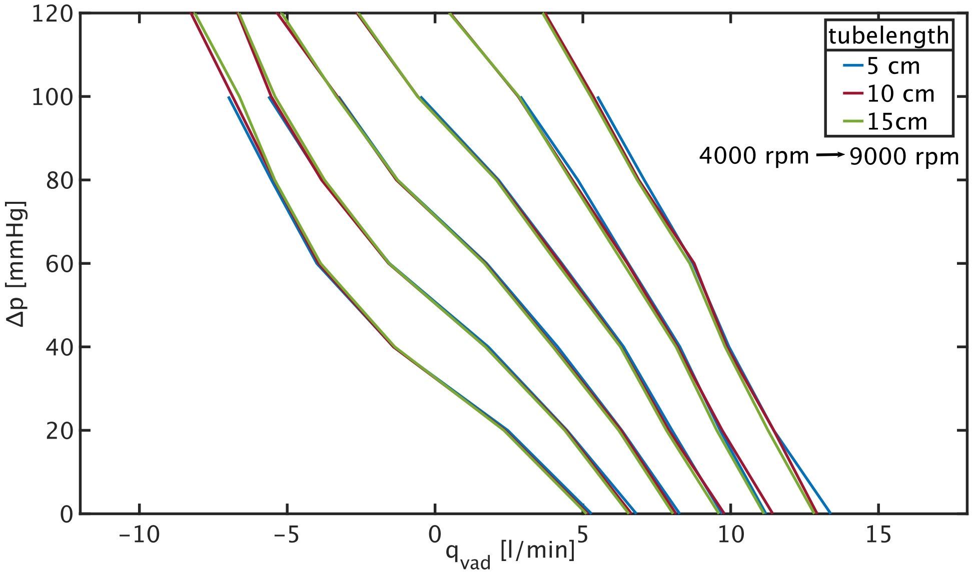

Figure 4.5: Static map for varying tube length in 60 % water 40 % glycerin solution.

The same measurements for determining the static map are performed in pure water, a solution of 80 % water 20 % glycerin, a solution of 60 % water 40 % glycerin and a solution of 40 % water 60 % glycerin. Representing the static maps for all four solutions measured, Figure 4.6 discloses significant deviations between the fluids.
Since resistance of the liquid falls with decreasing proportion of glycerin in the solution, differences in reachable differential pressure occur due to the aforementioned reason of spontaneous increase in backflow. However, as fluid resistance increases, pumpable flow decreases. All further measurements of this thesis are performed for a solution of 60 % water 40 % glycerin as this mixture most closely reflects the standard properties of blood. Figure A.1 to Figure A.3 in the appendix show comparisons of the static maps for varying tube length in different mixing ratios of water and glycerin and Figure A.4 and Figure A.5 depict comparisons of the static maps for varying solutions with 5 cm and 10 cm tube length. The resulting static map for the chosen final setup of the MCL is depicted in Figure 4.7.

As part of the system identification, the transfer function of the Sputnik VAD is determined. For this purpose, the step response of the pump to a 1000 rpm step in reference speed is analyzed.

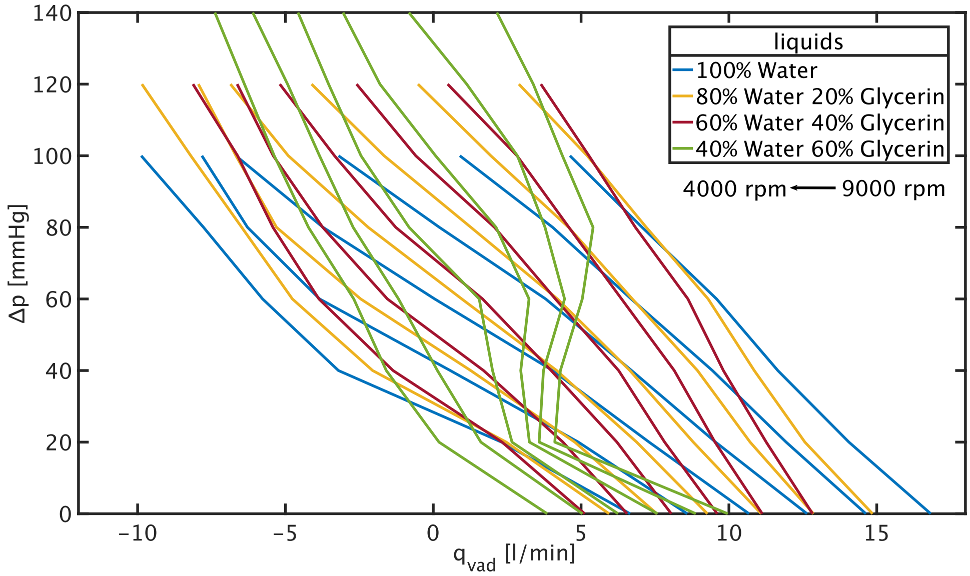

Figure 4.6: Static map for varying fluid solutions with $15\,cm$ long tubes.

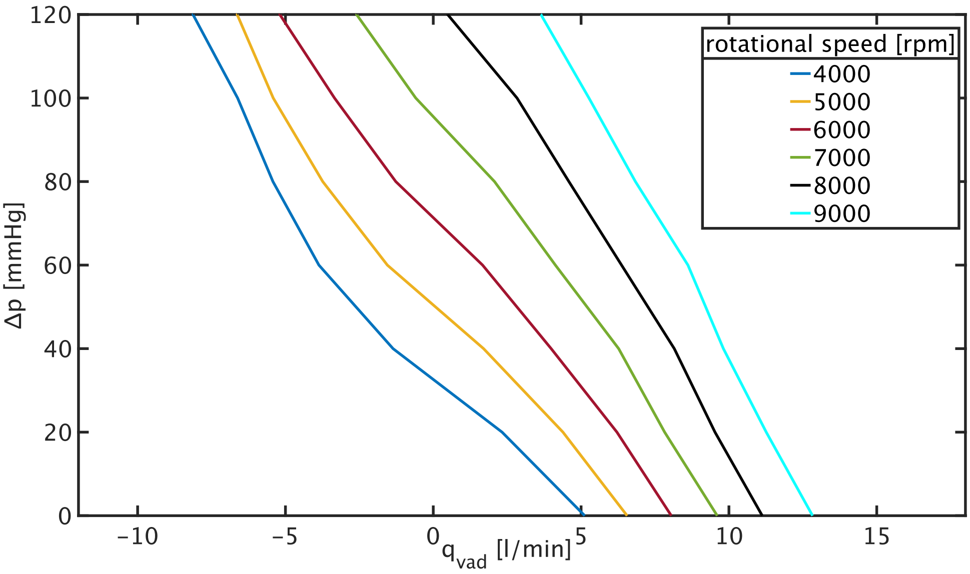

Figure 4.7: Static map for solution of $60\,\%$ water $40\,\%$ glycerin with $15\,cm$ long tubes.

Initially, the measured flow values from the static map determination measurement are prepossessed by using a 2^{nd}-order butterworth filter with a cut off frequency of $f_c = 5\,Hz$ and sampling frequency $f_s = 1000\,Hz$. For determination of the transfer function, filtered flow for an increase from $v_{\text{ref,low}} = 5000\,rpm$ to $v_{\text{ref,high}} = 6000\,rpm$

in reference speed at a differential pressure of $\Delta p = 40\,mmHg$ is analyzed. The blue line in Figure 4.8 depicts the filtered flow for this measurement. It is evident that the system's behavior can be approximated by a PT_1-element. The characteristic parameters of the transfer function according to equation (3.3) are also represented in Figure 4.8. The static gain k_s is determined as

$$k_\mathrm{s} = \frac{k_\mathrm{high} - k_\mathrm{low}}{v_\mathrm{ref,high} - v_\mathrm{ref,low}} = 0.0018 \tag{4.2}$$

with $k_\mathrm{high} = 2.3008$ and $k_\mathrm{low} = 0.4672$. The time constant T, defined as the time span between initialization of the jump and reaching $0.63 \cdot k_s$, is determinded to $T = 0.081\,s$. According to equation (3.3) the transfer function for the plant results in

$$G(s) = \frac{0.0018}{1 + 0.081s}. \tag{4.3}$$

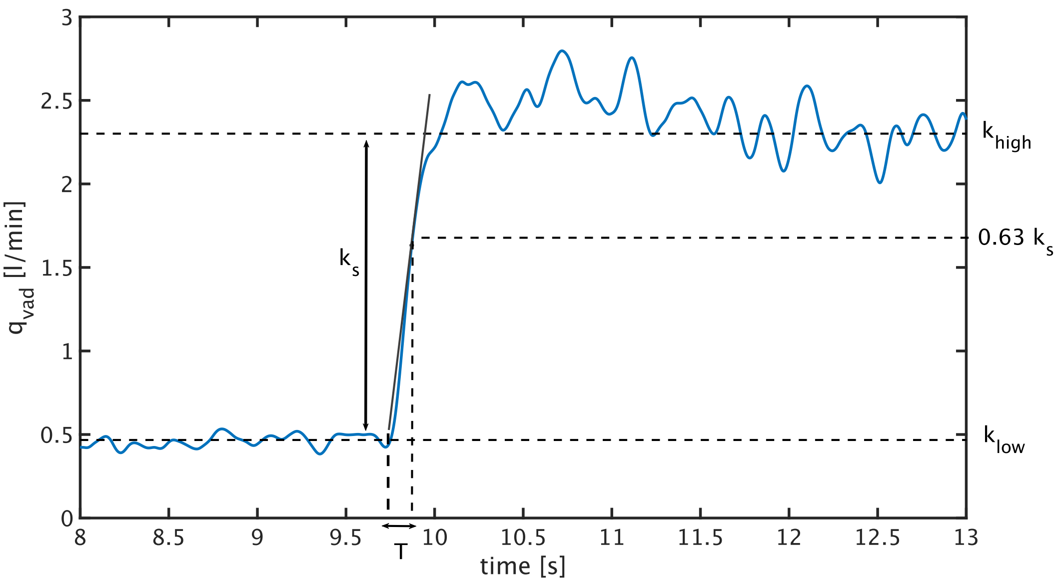

Figure 4.8: Step in flow, triggered by a step in reference speed by $1000\,rpm$ with identification of the variables for determining the transfer function of a PT_1 element.

In order to gain knowledge on the linearity of the system, the same analysis is performed for various differential pressure levels increased in steps of $20\,mmHg$ starting at $\Delta p = 0\,mmHg$ ending at $\Delta p = 120\,mmHg$. An overview on the characteristic values T, k_high, k_low and k_s is given in Table 4.2.

$\Delta p[mmHg]$	$T[s]$	$k_{\mathrm{high}}[l/min]$	$k_{\mathrm{low}}[l/min]$	$k_{\mathrm{s}}[l/min]$
0	0.139	6.7068	5.3303	0.0014
20	0.104	2.877	2.0198	$8.5786 \cdot 10^{-4}$
40	0.081	2.3008	0.4672	0.0018
60	0.108	1.6036	-1.303	0.0029
80	0.08	-0.9019	-3.0695	0.0022
100	0.0046	-2.6497	-4.2645	0.0016
120	0.096	-3.8616	-5.5587	0.0017

Table 4.2: Characteristic parameters for jumps of $1000\,rpm$ through the operating range of differential pressure.

Comparing the values of the differential pressure levels with each other, it can be seen that they are close to each other with the exception of three values: the static gain in the range of $\Delta p = 20\,mmHg$ and the time constants for $\Delta p = 0\,mmHg$ and $\Delta p = 100\,mmHg$. These deviations can be attributed at least in part to the high noise content in the signal and the filtering that is therefore necessary before determining the parameters. An assumption of linearity of the system is therefore regarded as admissible for the entire operating range.

5 Flow Control

In this chapter, implementation and evaluation of various control algorithms for flow control purposes will be presented. At first, the aim is to enable regulation of flow to a constant value. Later on, the system's ability to follow different reference flow trajectories is tested. In a final step, the system is subjected to disturbances through the HiL test rig in form of heart beats at different heart rates. Performances of the implemented control algorithms are compared.

5.1 PI Controller

PI control implementation is performed on the basis of the tuning rules according to Ziegler Nichols as well as according to Chien Hrones Reswick (Chapter 3.2.1). The performance of both controllers is later on compared and evaluated.

5.1.1 Design and Implementation

Prior to employing the inflection tangent method for these tuning approaches, a measurement similar to the one for determining the static map is performed. Figure 5.1 depicts the signal curves for determination of the tuning parameters. As presented in the upper graph, differential pressure is increased in steps of $20\,mmHg$ from $\Delta p = 0\,mmHg$ to $\Delta p = 100\,mmHg$. For each level, the sequence of reference velocities depicted exemplary for $\Delta p = 40\,mmHg$ in the center graph of Figure 5.2 is targeted. Starting at $v_{\text{ref}} = 4000\,rpm$, the velocity is first increased in three steps of varying height and then decreased by the same values. The first step amounts to $200\,rpm$, the second to $400\,rpm$ and the third to $600\,rpm$. The reference value is then increased by $1000\,rpm$ and again the three steps are executed. This sequential behavior is repeated up to a start value of $v_{\text{ref}} = 8000\,rpm$. To determine the parameters for controller design, the step from $v_{\text{ref,low}} = 5000\,rpm$ to $v_{\text{ref,high}} = 5400\,rpm$ at $\Delta p = 40\,mmHg$, which is located in the center of the pump's operating range, is

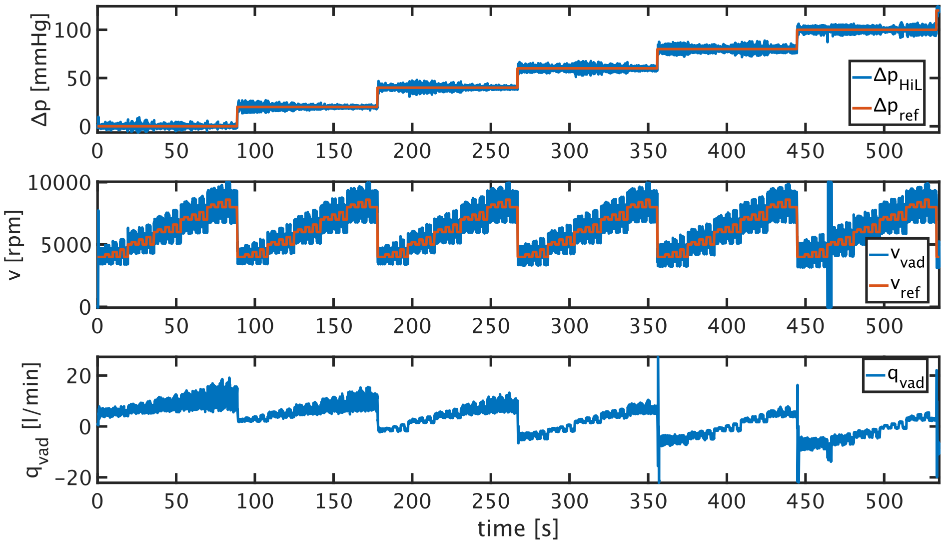

Figure 5.1: Signal curves for determination of PI controller parameters. Top: differential pressure as reference and measured signal, middle: reference and measured rotational speed, bottom: measured flow through Sputnik VAD.

used. This step is chosen for controller tuning as it allows for clear determination of the characteristic parameters k_{s}, T_{g} and T_{v}. Since the flow signal, however, is affected by high measurement noise, the signal is preprocessed using an 8^{th}-order butterworth filter with cut off frequency $f_{\mathrm{c}} = 5\,Hz$ and sampling frequency $f_{\mathrm{s}} = 1000\,Hz$. The resulting signal and the characteristic parameters needed for parameter tuning of the PI controller are depicted in Figure 5.3. With $k_{\mathrm{high}} = 2.8149$ and $k_{\mathrm{low}} = 1.7783$, the static gain is determined as in equation (4.2) to

$$k_{\mathrm{s}} = \frac{k_{\mathrm{high}} - k_{\mathrm{low}}}{v_{\mathrm{ref,high}} - v_{\mathrm{ref,low}}} = 0.0026. \tag{5.1}$$

The time constants amount to $T_{\mathrm{g}} = 0.193$ and $T_{\mathrm{v}} = 0.1$.
For tuning the PI controller according to Ziegler Nichols, equations (3.11) to (3.13) are used. K_{P} is, therefore, determined as

$$K_{\mathrm{P}} = 0.9 \cdot \frac{0.193}{0.0026 \cdot 0.1} = 670.3052 \tag{5.2}$$

and K_{I} as

$$K_{\mathrm{I}} = \frac{670.3052}{3.3 \cdot 0.1} = 2031.2278. \tag{5.3}$$

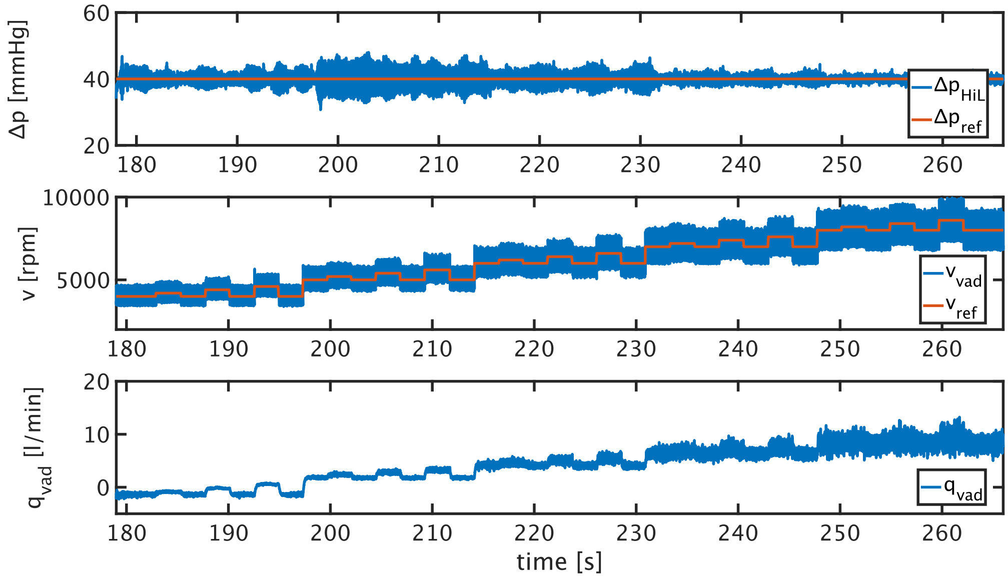

Figure 5.2: Signal curves for determination of PI controller parameters at $\Delta p = 40\,mmHg$.

Substituting these values in equation (3.10) results in the transfer function

$$G_{\mathrm{PI,ZN}}(s) = 670.3052 + \frac{2031.2278}{s}. \tag{5.4}$$

Overdamped controller behavior was chosen for controller tuning using Chien Hrones Reswick. Determination of the parameters K_{P} and K_{I} is performed following the equations presented in Table 3.1, resulting in

$$K_{\mathrm{P}} = 0.35 \cdot \frac{0.193}{0.0026 \cdot 0.1} = 260.6742 \tag{5.5}$$

and

$$K_{\mathrm{I}} = \frac{260.6742}{1.2 \cdot 0.1} = 2172.2853. \tag{5.6}$$

This in turn leads to the transfer function

$$G_{\mathrm{PI,CHR}}(s) = 260.6742 + \frac{2172.2853}{s}. \tag{5.7}$$

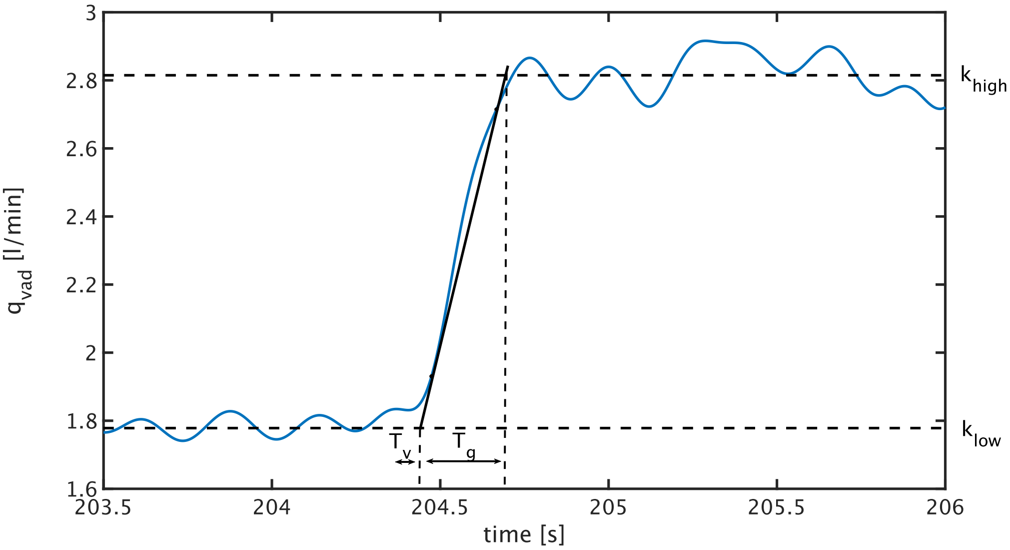

Figure 5.3: Step response for a step in rotational speed of 400 rpm for determination of PI controller tuning parameters.

5.1.2 Evaluation

The main purpose for employing a PI controller is to help improve the system's ability to suppress non repeating disturbances. Both controllers are tested under the same operating conditions and their performance is compared.
Even though the controllers are tuned at $\Delta p = 40\,mmHg$, both of them are tested in the differential pressure operating range from $\Delta p = 0\,mmHg$ to $\Delta p = 100\,mmHg$ to ensure sufficient performance in all use cases. For each differential pressure level, three consecutive steps up and down throughout the operating range of flow are performed. Each reference flow is targeted for 5 s and flow through the VAD is measured. A graphical representation of the reference signal curves is depicted in Figure 5.4. Figure 5.5a depicts the differential pressure and flow reference values, the measured pressure and flow value and the actuation variable in form of the reference rotational speed v_{act} and rotational speed of the VAD v_{vad} for the differential pressure level $\Delta p = 40\,mmHg$ using the PI controller tuned according to Ziegler Nichols, while Figure 5.5b depicts the same for the PI controller tuned according to Chien Hrones Reswick.

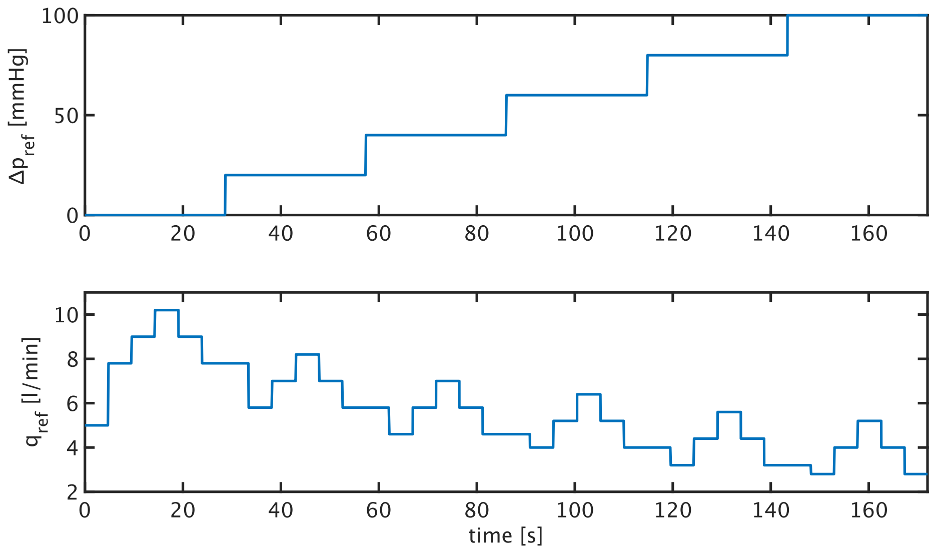

Figure 5.4: Reference signals for PI controller performance evaluation. Top: differential pressure reference value. Bottom: targeted flow trajectory.

The complete signal curves for the tests of the controllers are depicted in Figure A.6 and Figure A.7 in the appendix. Furthermore, the graphical representation of the test measurement at $\Delta p = 40\, mmHg$ for the controller tuned according to Ziegler Nichols is depicted in Figure A.8 of the appendix.

The course of the control error throughout the test measurements of the controller tuned according to Ziegler Nichols and the controller tuned according to Chien Hrones Reswick are depicted in Figure 5.6a and Figure 5.6b, respectively.

Throughout this work, to evalute controller performance, the root mean square error (RMSE) according to [CD14] defined as

$$RMSE = \sqrt{\frac{1}{n}\sum_{i=0}^{n} e_i^2} \tag{5.8}$$

is used. The RMSE for the differential pressure level of $\Delta p = 40\, mmHg$ for the Ziegler Nichols tuned controller amounts to

$$RMSE_{\mathrm{ZN},40} = 0.4013\, l/min \tag{5.9}$$

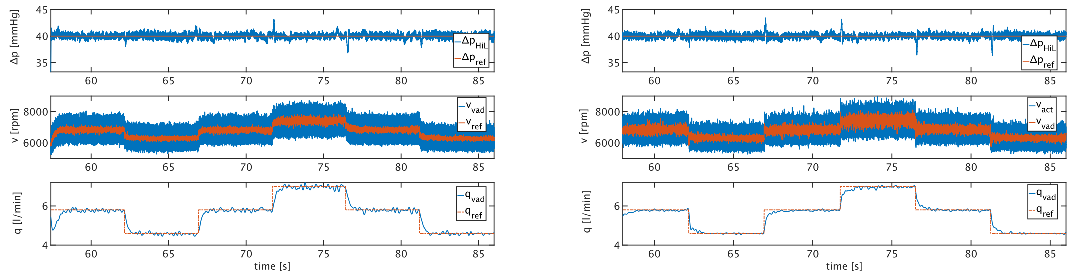

(a) **(b)**

Figure 5.5: Test measurements for PI controller at $\Delta p = 40\,mmHg$ tuned according to (a) Ziegler Nichols, (b) Chien Hrones Reswick.

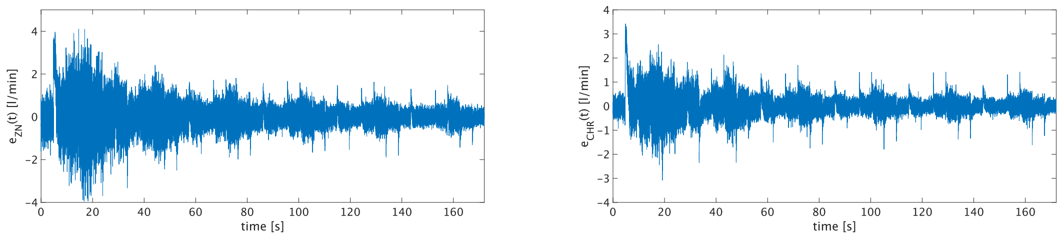

(a) **(b)**

Figure 5.6: Control error for PI controllers tuned according to (a) Ziegler Nichols, (b) Chien Hrones Reswick.

while the RMSE of the Chien Hrones Reswick tuned controller amounts to

$$RMSE_{\mathrm{CHR,40}} = 0.2753\,l/min. \tag{5.10}$$

Taking into account the full differential pressure operating range for RMSE calculation, these values amount to

$$RMSE_{\mathrm{ZN}} = 0.5396\,l/min \tag{5.11}$$

and

$$RMSE_{\mathrm{CHR}} = 0.3705\,l/min. \tag{5.12}$$

Comparing these results, it is evident that both controllers perform more precisely in the range of $\Delta p = 40\,mmHg$ for which tuning has been performed. Performance of the controller tuned according to Chien Hrones Reswick surpasses the Ziegler Nichols tuned one in both ranges. RMSE values for full range CHR control even indicate a higher performance in comparison to the Ziegler Nichols tuned controller in the range of $\Delta p = 40\,mmHg$. Due to its higher performance, for all following measurements the PI controller tuned in accordance to Chien Hrones Reswick is used.

5.2 Iterative Learning Control

As shown in Figure 5.5b, the exclusive use of a PI controller for flow control leads to necessity of measurement times of at least $1.5\,s$ to allow the flow to settle at a new reference value. However, one goal of this thesis is to enable flow control following different reference trajectories which may imply the need for faster reference tracking. By implementing an ILC approach, the necessary reduction of settling time, by gaining information from error values of the preceding iteration, will be made possible.

5.2.1 Design and Implementation

During this work a P-type ILC is implemented and optimized.
The implementation is based on a parallel architecture as depicted in Figure 3.6. This leads to the basic learning function for this ILC being given by

$$u_{\mathrm{j+1}}(k) = u_{\mathrm{j}}(k) + k_{\mathrm{p}} e_{\mathrm{j}}(k). \tag{5.13}$$

The learning gain k_{p} is experimentally chosen as

$$k_{\mathrm{p}} = 225 \tag{5.14}$$

to ensure quick error convergence.
As described in chapter 3.3, the basic ILC is extended to include a Q-filter to enable more precise tuning of the ILC and increase its robustness. This expansion results

in the learning function being described by

$$u_{j+1}(k) = Q(q)[u_j(k) + k_p e_j(k)]. \tag{5.15}$$

The Q-filter is implemented as a 2^{nd}-order butterworth filter with sampling frequency $f_s = 1000\,Hz$. The cut off frequency f_c is set to several values in order to compare and thus optimize performance and robustness of the iterative learning control system.
An additional part of the implementation is the generation of a repeating reference and a trigger signal. The trigger signal indicates the beginning of each new iteration and thus initiates calculation of the new values $u_{j+1}(k)$ in the ILC block. Figure 5.7 depicts three iterations of the reference signal for this ILC.
The signal is created by first generating a square wave signal with the upper stage at $6\,l/min$ and the lower stage at $4\,l/min$. Thus, the signal encloses the average value of $5\,l/min$ of the cardiac output of a healthy heart. The reference values are each held for $0.5\,s$, so that a complete iteration would correspond to a heart rate of 60 *beats per minute* (*bpm*). To avoid abrupt transitions in flow, possibly resulting in pump malfunctions, the reference signal was filtered with a 1^{st}-order Butterworth filter with cut off frequency $f_c = 20\,Hz$ and sampling frequency $f_s = 1000\,Hz$, resulting in radiused transitions. Afterwards, the signal is shifted by $0.25\,s$ to avoid placing the beginning of the test measurements at a jump point of the reference signal. The trigger signal is set from 0 to 1 at the beginning of each iteration for the duration of one sample.

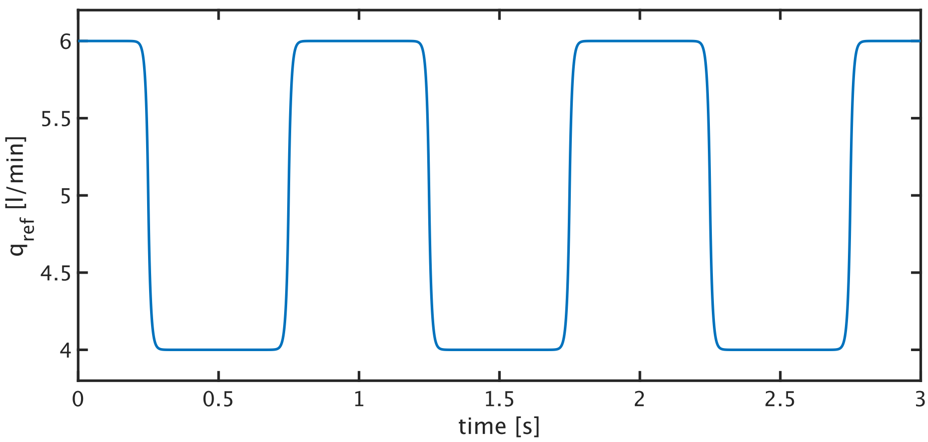

Figure 5.7: Three iterations of smoothed reference signal for ILC tuning.

5.2.2 Evaluation

As mentioned above, various cut off frequencies for the Q-filter of the ILC are tested with the aim of optimizing the ILC's performance and robustness.
The test signal for this purpose is given by repeatedly presenting the reference signal from Figure 5.7 to the system over a duration of $600\,s$. During the first $60\,s$, exclusive PI control is activated. This enables stable system performance at the beginning of ILC control. After these $60\,s$, the trigger signal sets off indications for beginnings of new iterations. From this point, ILC and PI controller are working simultaneously. During the complete test measurement, differential pressure is set to $\Delta p = 40\,mmHg$. Measurements with this setup are performed for cut off frequencies $f_\mathrm{c} = 8\,Hz$, $f_\mathrm{c} = 20\,Hz$, $f_\mathrm{c} = 25\,Hz$ and $f_\mathrm{c} = 34\,Hz$.
Figure 5.8 exemplifies a sequence of the measurement performed for the Q-filter set to a cut off frequency of $f_\mathrm{c} = 8\,Hz$. The segment shows the transition from exclusive PI control to the parallel control structure of PI control and ILC. The upper graph depicts the measured differential pressure at the MCL. The spikes in this curve occur due to varying flow through the blood pump resulting in changing volumes inside the pressure chambers. The middle graph represents the rotational speed values for the actuating variable v_act and the actual velocity of the pump's rotor v_vad.

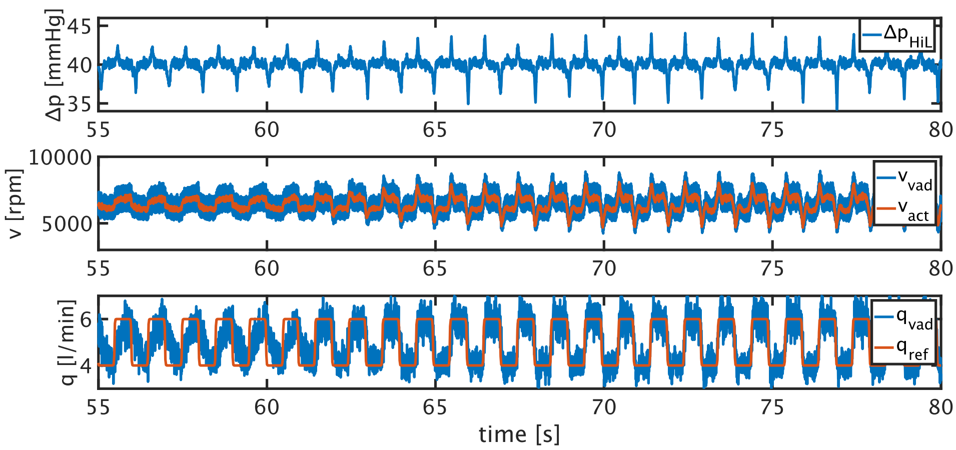

Figure 5.8: Test measurement for ILC at cut off frequency $f_\mathrm{c} = 8\,Hz$. Top: differential pressure value of the MCL. Middle: actuating variable and measured rotational speed of the VAD. Bottom: targeted flow trajectory and measured flow through the VAD.

The bottom graph of Figure 5.8 depicts the reference flow trajectory q_{ref} and the measured flow q_{vad} that is conveyed by the VAD. Looking at this curve, it can be seen that by solely using the PI controller (corresponding to $55\,s$ to $60\,s$ of the graph), the flow through the VAD cannot be adjusted fast enough and thus the reference trajectory cannot be followed successfully. However, from the onset of the ILC at about $60\,s$, it can be seen that the measured flow continues to adapt to the given reference flow within a few iterations.

The measurement with $f_{\mathrm{c}} = 20\,Hz$ as cut off frequency of the Q-filter shows stable behavior over the complete measurement time, similar to the measurement performed with $f_{\mathrm{c}} = 8\,Hz$.

While the system shows stable behavior over the complete measurement time for cut off frequencies of $f_{\mathrm{c}} = 8\,Hz$ and $f_{\mathrm{c}} = 20\,Hz$, in case of $f_{\mathrm{c}} = 25\,Hz$ the system shows oscillatory behavior. Figure 5.9 depicts part of the measurement for a cut off frequency set to $f_{\mathrm{c}} = 25\,Hz$.

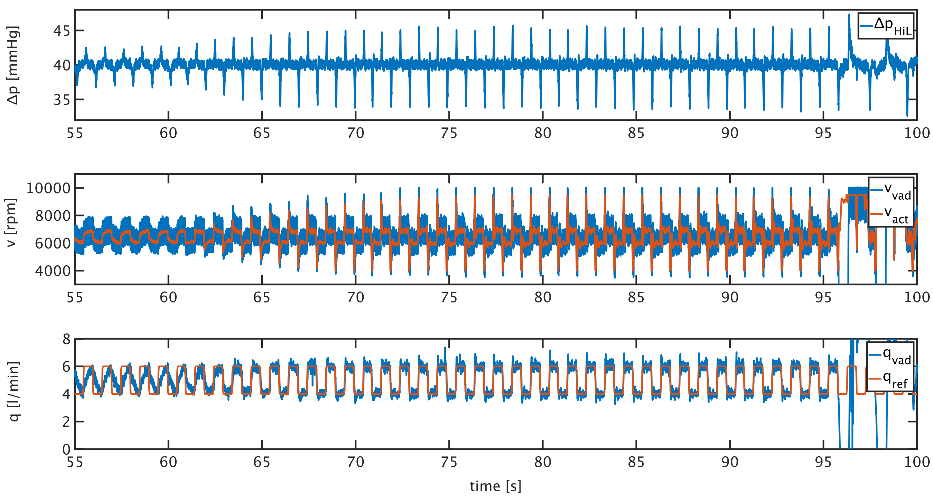

Figure 5.9: Test measurement for ILC at cut off frequency $f_{\mathrm{c}} = 25\,Hz$. Top: differential pressure value of the MCL. Middle: actuating variable and measured rotational speed of the VAD. Bottom: targeted flow trajectory and measured flow through the VAD.

The structure is the same as for Figure 5.8. However, in this case, looking at the middle graph, it is evident that with each additional ILC iteration the actuation variable v_{act} rises further towards its saturation values $4000\,rpm$ and $9000\,rpm$. This ultimately leads to the pump's rotor to stop, due to abrupt changes in speed and

flow at approximately 96 s measurement time.
Behavior of the system for a cut off frequency set to $f_c = 34\,Hz$ is similar to behavior with $f_c = 25\,Hz$. The oscillatory system behavior again results in the pump's rotor to stop at approximately 98 s.
In order to determine which cut off frequency is most suited for the ILC implementation, the RMSE values of the iterations for each of the measurements are compared to another. Figure 5.10 depicts the RMSE of each measurement as a function of the iteration for the first 39 iterations of the ILC. The figure also represents the RMSE value of exclusive PI control in form of the first iteration value:

$$RMSE_{PI} = RMSE(1) = 0.85\,l/min \tag{5.16}$$

It is evident that the curves for $f_c = 25\,Hz$ and $f_c = 35\,Hz$ show abrupt increases in RMSE for the iterations when the pump stopped. Due to this unstable behavior, these cut off frequencies are not suitable for ILC implementation.

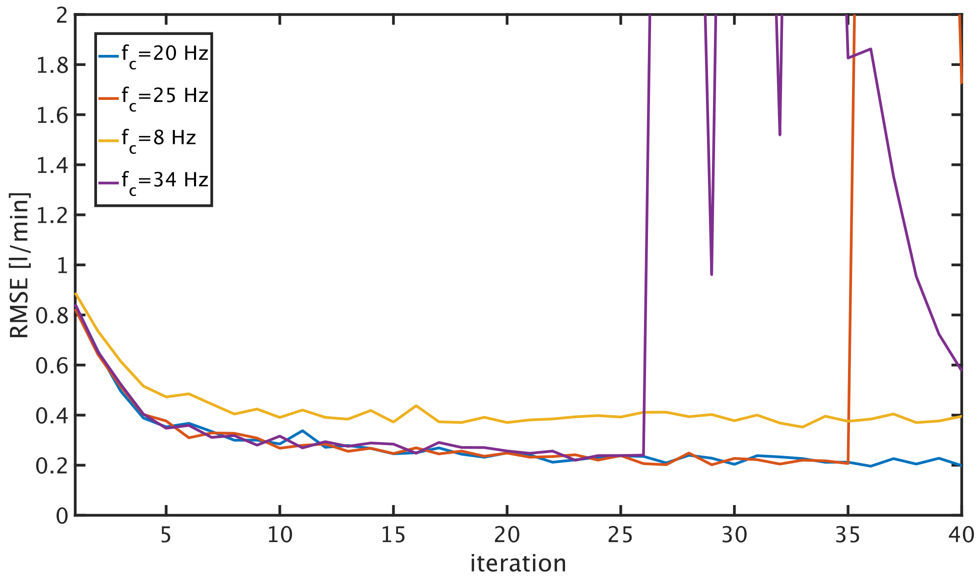

Figure 5.10: Comparison of RMSE values for different cut off frequencies of ILC Q-filter.

Comparing the RMSE values of the 39th iteration of the other two frequencies, it is clear that performance of the ILC with Q-filter cut off frequency at $f_c = 20\,Hz$ with

$$RMSE_{f_c=20\,Hz}(39) = 0.1984\,l/min \tag{5.17}$$

is higher than for $f_\mathrm{c} = 8\,Hz$ with

$$RMSE_{\mathrm{f_c=8\,Hz}}(39) = 0.3951\,l/min. \tag{5.18}$$

Therefore, the cut off frequency of the Q-filter in all following measurements will be set to $f_\mathrm{c} = 20\,Hz$.

As these measurements only took into account a differential pressure value of $\Delta p = 40mmHg$, the ILC with the optimized Q-filter cut off frequency is tested at pressure levels in equal steps of $20\,mmHg$ between $\Delta p = 20mmHg$ and $\Delta p = 80\,mmHg$ to ensure stable system behavior in all operating points. For this, the same measurement as before is executed.
A comparison of the RMSE values over all iterations of the ILC for the four differential pressure levels is depicted in Figure 5.11. The course of the RMSE values of all four measurements indicate stable system behavior. With values of approximately $0.3\,l/min$, the RMSE of the other operating points is only slightly higher than of the $40\,mmHg$ operating point with an RMSE of approximately $0.2\,l/min$. Therefore, the implemented ILC is suitable for all of the tested operating points.

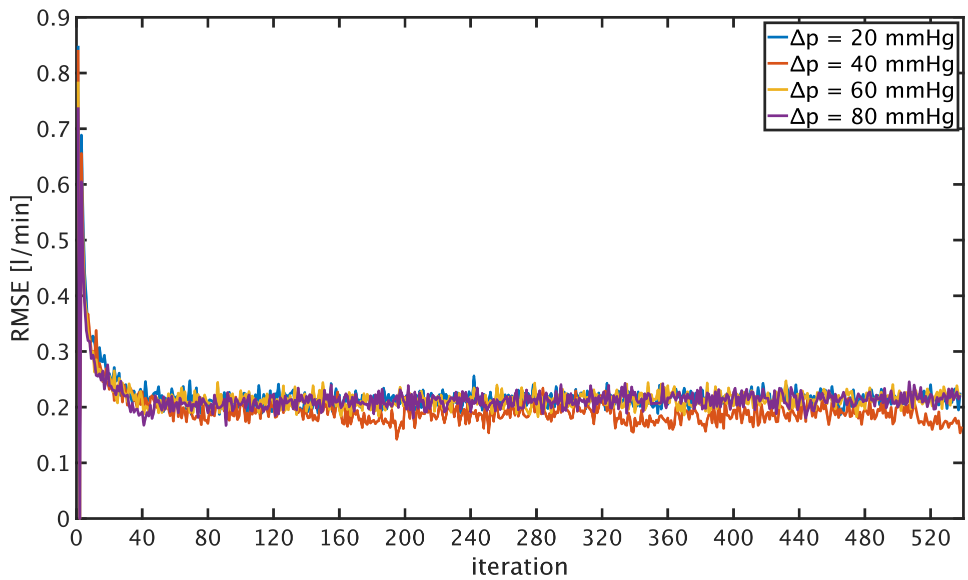

Figure 5.11: Comparison of RMSE values of the ILC at different differential pressure operating points.

5.3 Iterative Learning Control with repeating disturbance

The ILC implemented in the previous section was tested and optimized under idealized conditions without being influenced by any disturbances. Since in real use, the VAD is exposed to disturbances by pressure changes due to the beating of the heart, this section aims to include this influence into the measurements by use of the circulatory system simulator's functionality to simulate the heart beat including anticipated pressure changes.

Initially, only repeating disturbances are taken into account as the standard P-type ILC used is only setup to compensate these. The MCL is used to introduce the setup to a disturbance in form of heart beats at a constant heart rate. Including the influence of the heart beat as a disturbance requires changing the trigger signal from a manually programmed one to using the start of each heart beat as the trigger of new iterations.

5.3.1 Reference trajectories

Testing of the ILC subjected to repeating disturbances is performed for several reference flow trajectories. These trajectories are generated using Matlab and are selectable during runtime via ControlDesk through the use of an indicator variable.

As a first reference, the flow is set to a constant value of $q_{\mathrm{ref}} = 5\,l/min$. By this, the controller's ability to balance out the pressure fluctuations during a heart beat is tested.
The second signal, which is used as a reference trajectory, is a sinusoidal signal that oscillates around a value of $4\,l/min$, has a maximum value of $5\,l/min$ and a minimum value of $3\,l/min$. One iteration of this signal is set to $1\,s$, matching a $60\,bpm$ heart rate. The signal course is depicted as a blue line in Figure 5.12.

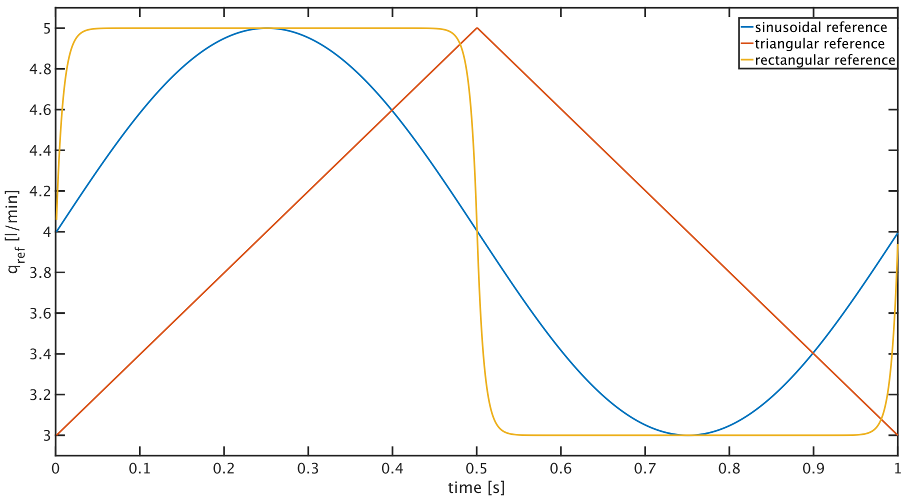

Figure 5.12: Sinusoidal reference signal.

The third reference trajectory is given in form of a triangular signal. As for the sinusoidal signal, the maximum value is set to $q_{\text{ref}} = 5\,l/min$ and the minimum to $3\,l/min$. Again the full signal length is set to $1\,s$ to match a $60\,bpm$ heart rate. The red line of Figure 5.12 depicts one iteration of the reference trajectory.
As a last trajectory, a rectangular signal similar to the one used in chapter 5.2 is chosen. The upper step is set to $q_{\text{ref}} = 5\,l/min$ and the lower one to $q_{\text{ref}} = 3\,l/min$. Both are held for $0.5\,s$. Again, the signal is filtered using a 1^{st} order butterworth filter with cut off frequency $f_{\text{c}} = 20\,Hz$ and sampling frequency $f_{\text{s}} = 1000\,Hz$.
The yellow line in Figure 5.12 depicts one iteration of the reference.

5.3.2 Evaluation

Using the reference trajectories described above, several measurements are performed and evaluated to determine performance of the ILC subjected to repeating disturbances. Measurements are performed for varying levels of contractility of the left ventricle for all reference trajectories. The performance results of the contractility levels are compared to each other. Contractility is decreased in steps of 0.25 from $cf_{\text{Lv}} = 1$ representing contractility of a healthy heart to $cf_{\text{LV}} = 0.25$ correlating to a severe impairment of heart functionality.

During all measurements for the first $120\,s$, PI control is activated exclusively to ensure stable system behavior at the beginning of additional ILC control.

In a first step, measurements are performed using the constant reference flow of $q_{\text{ref}} = 5\,l/min$. Figure 5.13 depicts the transition from exclusive PI control $(115 - 120\,s)$ to use of the parallel control structure $(120 - 130\,s)$ for a contractility of $cf_{\text{LV}} = 1$. It is evident that the PI controller alone is not able to suppress the disturbance's influence on the flow. As soon as ILC control sets in, the flow settles further towards the constant reference flow with each ILC iteration.

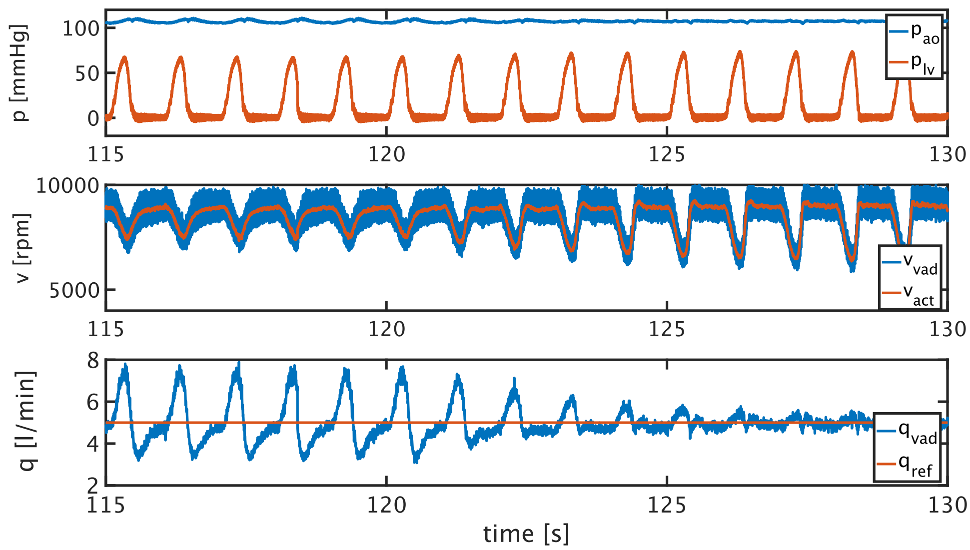

Figure 5.13: Segment of measurement for ILC with disturbance of $HR = 60\,bpm$ with $cf_{\text{Lv}} = 1$ for constant reference flow. Top: pressure values of the MCL. Middle: actuating variable and measured rotational speed of the VAD. Bottom: targeted flow trajectory and measured flow through the VAD.

Measurements for all contractility levels are running stable until the end of measurement time is reached at $600\,s$. A comparison of the RMSE values for each iteration is presented in Figure 5.14. Up to iteration 120, the graph represents the RMSE of the PI controller. For this time, it is evident that with decreasing left ventricular contractility, RMSE also decreases from $RMSE_{\text{PI,const,cf}_{\text{Lv}}=1} \approx 1.2\,l/min$ to $RMSE_{\text{PI,const,cf}_{\text{Lv}}=0.25} \approx 0.4\,l/min$. This can be explained by the lower influence of pressure changes due to weakened contractility. The RMSE values for all four contractility levels using combined PI and ILC control amount to

$$RMSE_{\text{ILC,const}} \approx 0.14\, l/min. \tag{5.19}$$

It is evident that using the combined control approach results in significantly higher performance in all contractility ranges for a constant reference flow.

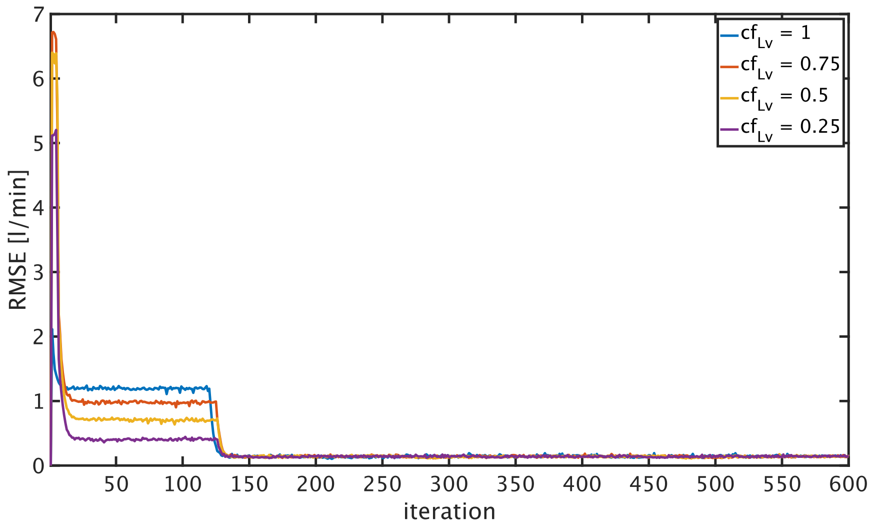

Figure 5.14: Comparison of RMSE values of the ILC for constant reference flow with disturbance of $HR = 60\, bpm$ for varying contractility values of the left ventricle.

The next measurements performed are the ones testing the controller's ability to follow the sinusoidal reference trajectory. The trajectory is placed synchronous to the heart beat. Figure 5.15 illustrates the transition phase from PI to combined control for the sinusoidal reference at $cf_{\text{Lv}} = 1$. Similar to the constant reference flow, the PI controller alone is not able to follow the reference trajectory. The combination between PI controller and ILC, however, leads to a clearly recognizable improvement of the following behavior within some iterations. The comparison of RMSE values (see Figure 5.16) leads to similar conclusions as for the constant reference flow. During the first 120 iterations when only PI control is active, the RMSE reduces with decreasing contractility of the left ventricle.

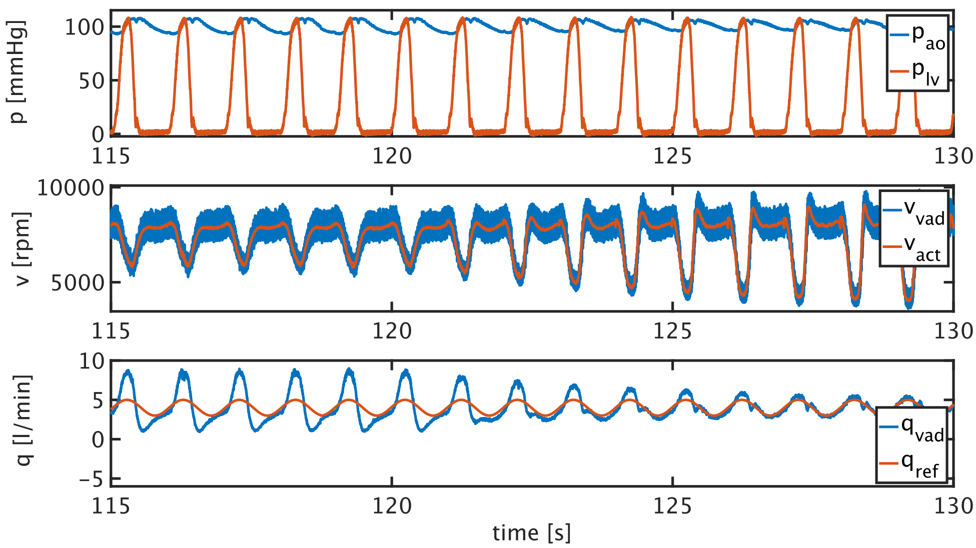

Figure 5.15: Segment of measurement for ILC with disturbance of $HR = 60\,bpm$ with $cf_{\mathrm{Lv}} = 1$ for sinusoidal reference flow. Top: pressure values of the MCL. Middle: actuating variable and measured rotational speed of the VAD. Bottom: targeted flow trajectory and measured flow through the VAD

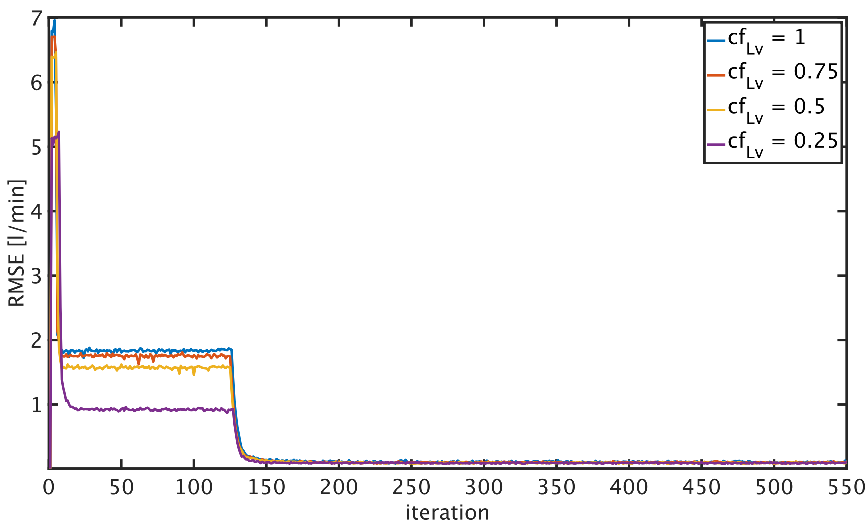

Figure 5.16: Comparison of RMSE values of the ILC for sinusoidal reference flow with disturbance of $HR = 60\,bpm$ for varying contractility values of the left ventricle.

However, the decrease between contractility values from $cf_{\mathrm{LV}} = 1$ to $cf_{\mathrm{LV}} = 0.75$ and $cf_{\mathrm{LV}} = 0.5$ with $RMSE_{\mathrm{PI,sine,cf_{Lv}=1}} \approx 1.85\,l/min$, $RMSE_{\mathrm{PI,sine,cf_{Lv}=0.75}} \approx 1.75\,l/min$

and $RMSE_{\mathrm{PI,sine,cf_{Lv}=1}} \approx 1.85\, l/min$, are less significant than the reduction of contractility to $cf_{\mathrm{Lv}} = 0.25$ with $RMSE_{\mathrm{PI,sine,cf_{Lv}=0.25}} \approx 0.93\, l/min$. Performance for the combined control approach is almost equal for all contractility values with

$$RMSE_{\mathrm{ILC,sine}} \approx 0.09\, l/min. \tag{5.20}$$

The absolute RMSE value indicates an increase in performance in all cases.

Measurement for the triangular reference trajectory shows slowly oscillating behavior for left ventricular contractility at $cf_{\mathrm{Lv}} = 1$ and $cf_{\mathrm{Lv}} = 0.75$. Figure 5.17, representing the measurement at $cf_{\mathrm{Lv}} = 1$, shows that from the onset of the ILC, initially, a clear approximation to the reference signal is achieved, but the actuating variable v_{act} (middle graph) continues to reach its saturation limits with each iteration. This ultimately leads to a stoppage of the pump.

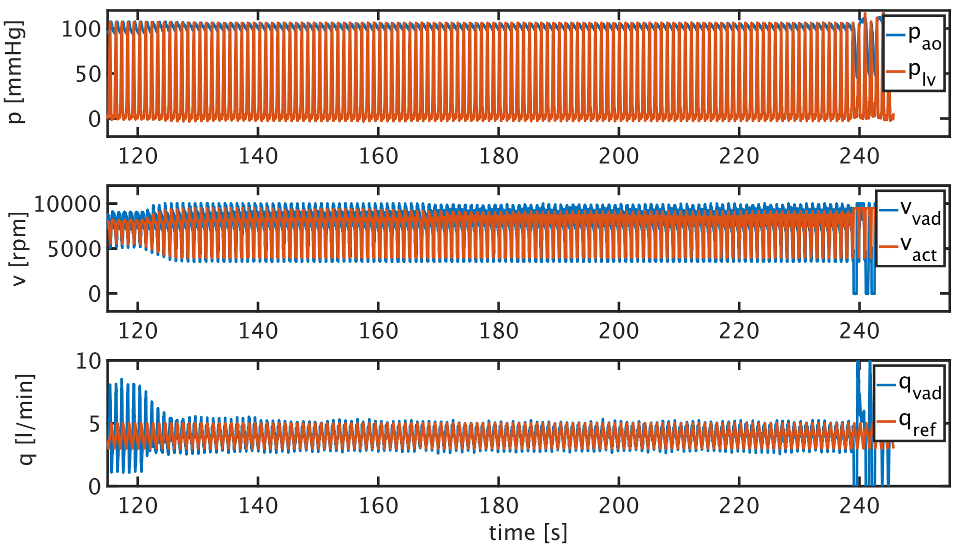

Figure 5.17: Measurement for ILC with disturbance of $HR = 60\, bpm$ with $cf_{\mathrm{Lv}} = 1$ for triangular reference flow. Top: pressure values of the MCL. Middle: actuating variable and measured rotational speed of the VAD. Bottom: targeted flow trajectory and measured flow through the VAD.

Measurements for contractility values $cf_{\mathrm{Lv}} = 0.5$ and $cf_{\mathrm{Lv}} = 0.25$ show stable behavior over the complete measurement time of $600\, s$. The transition segment for the measurement at $cf_{\mathrm{Lv}} = 0.5$ shown in Figure 5.18 again indicates an improved performance for the ILC.

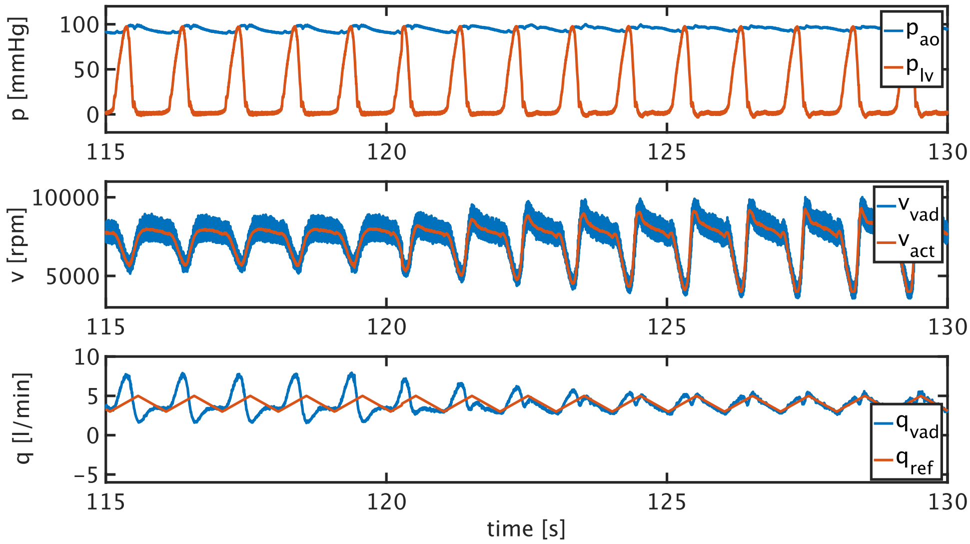

Figure 5.18: Segment of measurement for ILC with disturbance of $HR = 60\,bpm$ with $cf_{\mathrm{Lv}} = 0.5$ for triangular reference flow. Top: pressure values of the MCL. Middle: actuating variable and measured rotational speed of the VAD. Bottom: targeted flow trajectory and measured flow through the VAD.

This is endorsed by comparison of the RMSE values as shown in Figure 5.19. While RMSE for the PI controller segments lie at $RMSE_{\mathrm{PI,triang,cf_{Lv}=0.5}} \approx 1.9\,l/min$ and $RMSE_{\mathrm{PI,triang,cf_{Lv}=0.25}} \approx 1.2\,l/min$, the RMSE for the combined control structure amounts to

$$RMSE_{\mathrm{ILC,triang}} \approx 0.11\,l/min. \tag{5.21}$$

The last measurements for analysis of controller performance of the ILC subjected to a repeating disturbance are performed using the rectangular reference trajectory. As in all previous measurements, the exclusive use of the PI controller is not suitable to track the reference. Combined control, however, once more shows adjustment to the reference in a few iterations. Figure 5.20 depicts the course of pressure in the aorta and left ventricle, the actuating variable and the rotational speed of the VAD as well as the reference trajectory and the actually achieved flow through the VAD for the transitional segment of the measurement at $cf_{\mathrm{Lv}} = 1$.

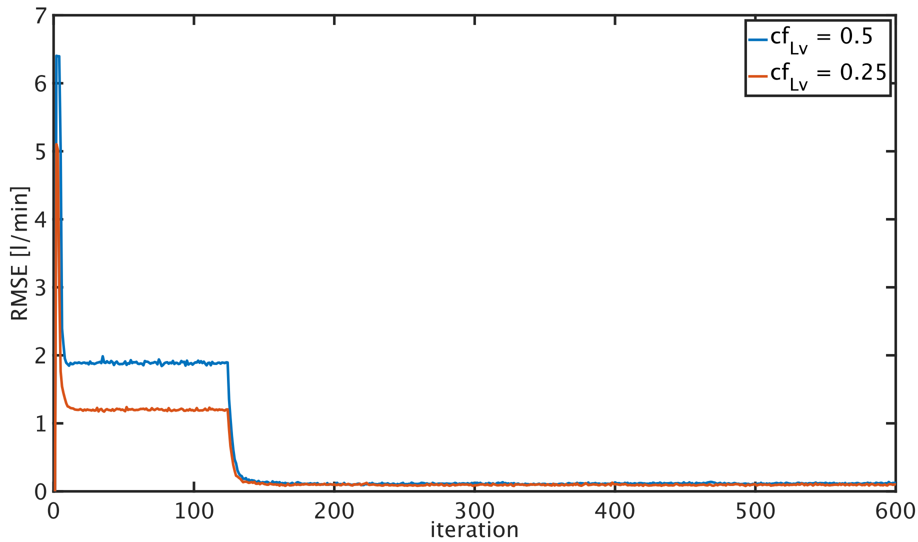

Figure 5.19: Comparison of RMSE values of the ILC for triangular reference flow with disturbance of $HR = 60\,bpm$ for varying contractility values of the left ventricle.

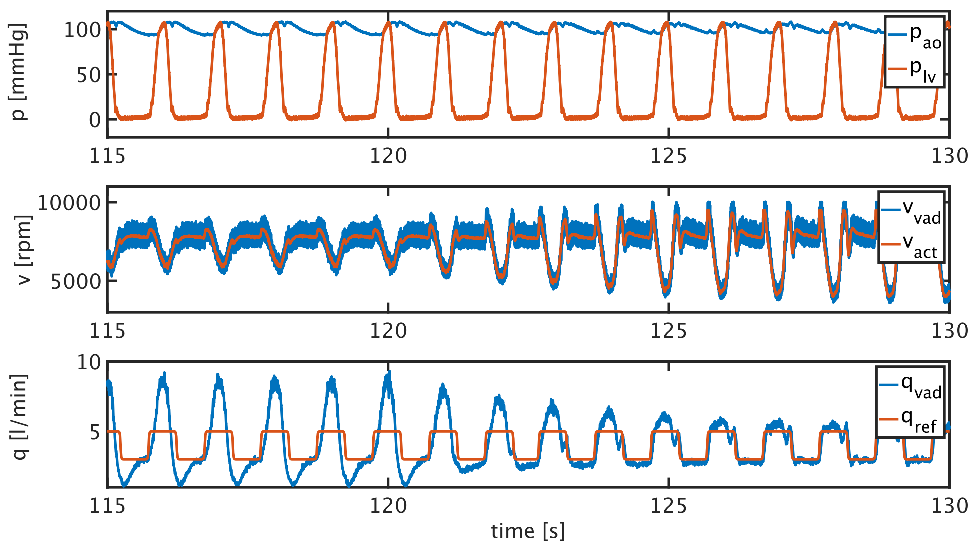

Figure 5.20: Segment of measurement for ILC with disturbance of $HR = 60\,bpm$ with $cf_{\mathrm{Lv}} = 1$ for rectangular reference flow. Top: pressure values of the MCL. Middle: actuating variable and measured rotational speed of the VAD. Bottom: targeted flow trajectory and measured flow through the VAD.

The comparison of RMSE courses for all four left ventricular contractility levels is depicted in Figure 5.21. Once more, contractility decrease directly influences the performance of the PI controller while the end value for RMSE of the ILC for all contractility levels amounts to

$$RMSE_{\text{ILC,rect}} \approx 0.22\, l/min. \tag{5.22}$$

To prepare measurements considering different disturbances, in addition to measure-

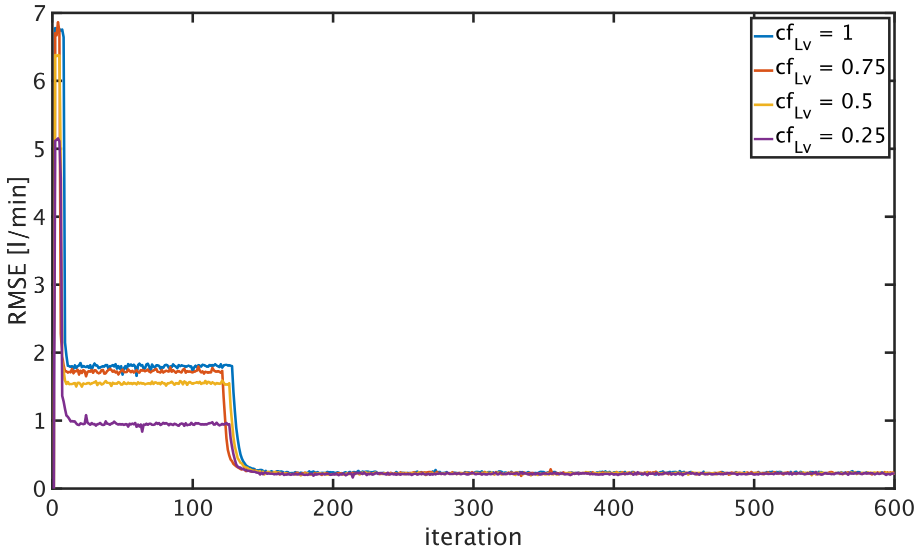

Figure 5.21: Comparison of RMSE values of the ILC for rectangular reference flow with disturbance of $HR = 60\, bpm$ for varying contractility values of the left ventricle.

ments considering different contractility values for the left ventricle, measurements are performed at several heart rates for the rectangular reference. Heart rate is defined in four steps of $20\, bpm$ from $HR = 40\, bpm$ to $HR = 100\, bpm$. All of these measurements show stable behavior throughout the complete measurement time of $500\, s$. Looking at Figure 5.22, it can be concluded that the performance of the PI controller improves only for the slowest heart rate of $HR = 40\, bpm$ compared to the rest. The results for the RMSE of the ILC control, however, show that with decreasing heart rate the RMSE value decreases continually from

$$RMSE_{\text{ILC,100bpm}} \approx 0.22\, l/min \tag{5.23}$$

to

$$RMSE_{\text{ILC,40bpm}} \approx 0.16\, l/min. \tag{5.24}$$

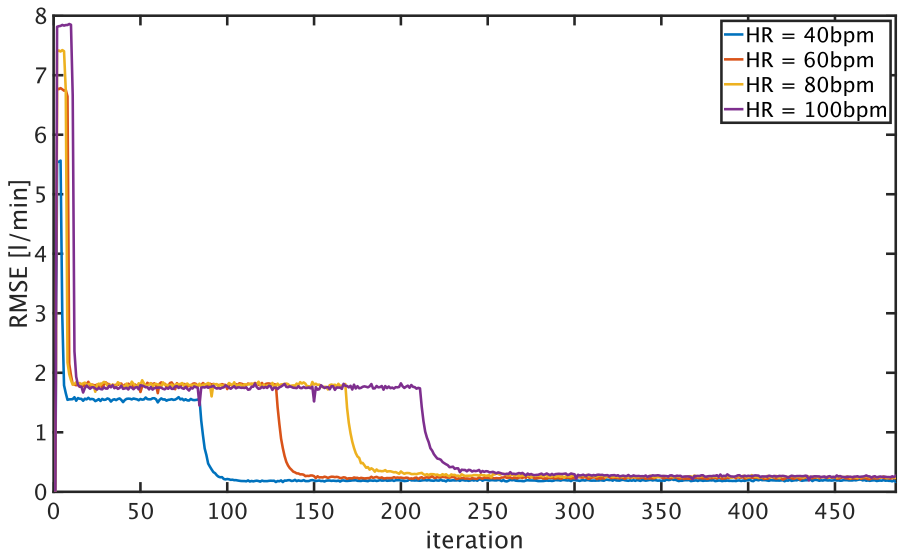

Figure 5.22: Comparison of RMSE values of the ILC for rectangular reference flow with $cf_{\text{Lv}} = 1$ for varying heart rates.

However, the results indicate that using ILC control is a suitable option for all of these heart rates.

5.4 Iterative Learning Control with varying disturbance

Due to the fact that a person's heartbeat does not always occur at a uniform heart rate but is subject to fluctuations, the ILC is tested for use in suppressing varying disturbances.

5.4.1 Design and Implementation

As the standard P-type ILC is not set up for use under the influence of non repeating disturbances, some changes have to be implemented.
To perform the tests under the influence of changing disturbances, an additional function programmed in Matlab is added to the Simulink model. This allows a constant variation of the heart rate. The function is designed in such a way that by receiving the trigger signal of a new heartbeat, a new heart rate is determined and passed on to the mock circulatory loop and the ILC. In addition to the trigger signal, the function has three more inputs in the form of an upper and lower limit of the heart rate and a step size for a variation of the heart rate. These variables can be set via ControlDesk before starting the measurement. Starting at the lower limit, the heart rate is increased by the defined step size with each heartbeat until the upper limit of the heart rate is reached. Then, with each heartbeat, the heart rate is decreased by the step size until the lower limit is reached. This is repeated until the measurement is stopped. An example of this sequence with a lower limit of 60 bpm, a step size of 1 bpm and an upper limit of 100 bpm is shown in Figure 5.23.

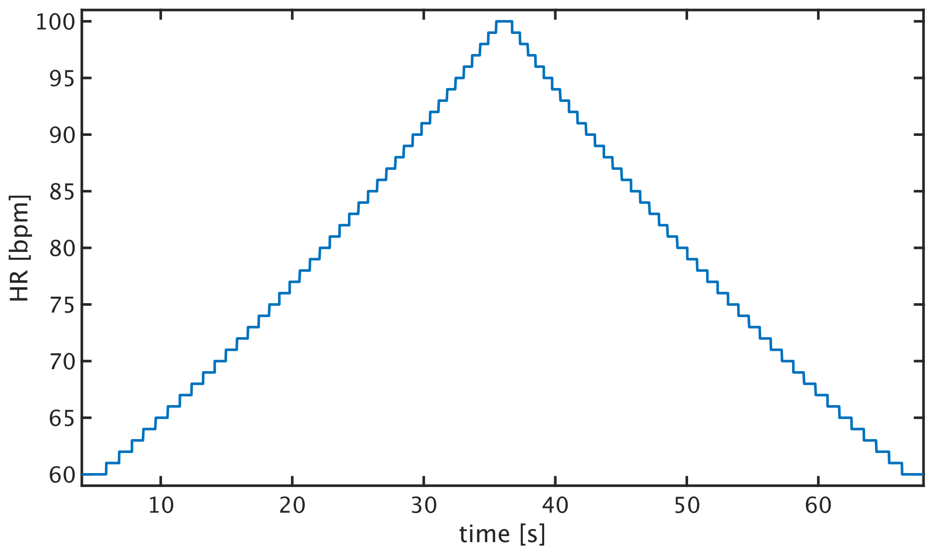

Figure 5.23: Illustration of HR change.

Since the variation of the heart rate leads to changing iteration duration, an additional preprocessing step is implemented within the ILC function. This introduces a functionality which allows to resample the stored data of the previous iteration and adapt it to the duration of the current iteration. This process is performed after the data filtering step of the ILC, before the data is output to the control loop.
To adjust resampling of the data to the length of the current iteration knowledge of the heart rates is required. Within the tests at the MCL, this requirement is fulfilled. For an application on the patient, an additional use of an ECG would be necessary. The resampling function calculates the iteration length according to

$$it\_len = \lfloor \frac{60}{HR} \cdot 1000 \rfloor \tag{5.25}$$

with HR being the heart rate. The duration of the last iteration is stored in the variable it_len_prev. Using this variable and the current iteration length, an index factor is calculated to

$$idx = \frac{it\_len\_prev}{it\_len}. \tag{5.26}$$

This factor is required to determine the indices of the stored actuating variable values which are to be used to calculate the new values. In the next step, the lengths of the last and current iteration are compared. In case the iteration times correspond to each other, the stored data are used unchanged for the output to the control loop

$$\mathbf{u}_{\mathrm{j,ILC}}(i) = \mathbf{u}_{\mathrm{j,ILC,prev}}(i) \tag{5.27}$$

for all entries i. $\mathbf{u}_{\mathrm{j,ILC,prev}}$ corresponds to the filtered data stored in the actuating variable memory during the last iteration while $\mathbf{u}_{\mathrm{j,ILC}}$ represents the data output during the current iteration.
Calculation steps for different iteration durations differ only for the first entry. In case the current iteration length is shorter than the last ($it\_len < it\_len\_prev$)

$$\mathbf{u}_{\mathrm{j,ILC}}(1) = \mathbf{u}_{\mathrm{j,ILC,prev}}(1) \tag{5.28}$$

is always valid for the first entry of the actuating variable. A weighting factor is required for all other entries i of the actuating variable vector to determine resampled data. This factor is calculated as

$$weight = i \cdot idx - \lfloor i \cdot idx \rfloor. \tag{5.29}$$

The value for the current entry i is then determined as

$$\mathbf{u}_{\mathrm{j,ILC}}(i) = (1 - weight) \cdot \mathbf{u}_{\mathrm{j,ILC,prev}}(\lfloor i \cdot idx \rfloor) + weight \cdot \mathbf{u}_{\mathrm{j,ILC,prev}}(\lceil i \cdot idx \rceil) \quad (5.30)$$

with $\lfloor\,\rfloor$ indicating rounding off the value and $\lceil\,\rceil$ indicating rounding up. Through this calculation, the data from the previous iteration is compressed or stretched to the current iteration length accordingly.

5.4.2 Evaluation

In order to determine whether resampling of data improves the ILC performance under varying disturbances, two sets of tests are performed: One without resampling the data under variable disturbances and one using the resampling function described above. The results of the tests are compared with each other. The reference trajectories described in section 5.3.1 are used to perform the measurements. All measurements considered here are performed assuming a left ventricular contractility of $cf_{\mathrm{Lv}} = 1$.

At first, a constant reference flow of $4\,l/min$ is presented to the system. Figure 5.24 depicts a segment of the measurement without resampling of the actuating variable data representing the transition from exclusive PI control to the combined control approach at $120\,s$. At about $152\,s$, the pump stops due to the steadily oscillating behavior of the actuating variable. As can be seen in Figure 5.25, similar behavior is observed for the measurement with the resampled actuating variable data. However, looking at the lower graphs of the two figures, it can be seen that for the unchanged actuating variable data in Figure 5.24, the measured flow q_{vad} first approaches the reference, but then moves further away from it again, while the flow through the VAD for the measurement with resampling of the actuating variable data in Figure 5.25 continuously approaches the reference.

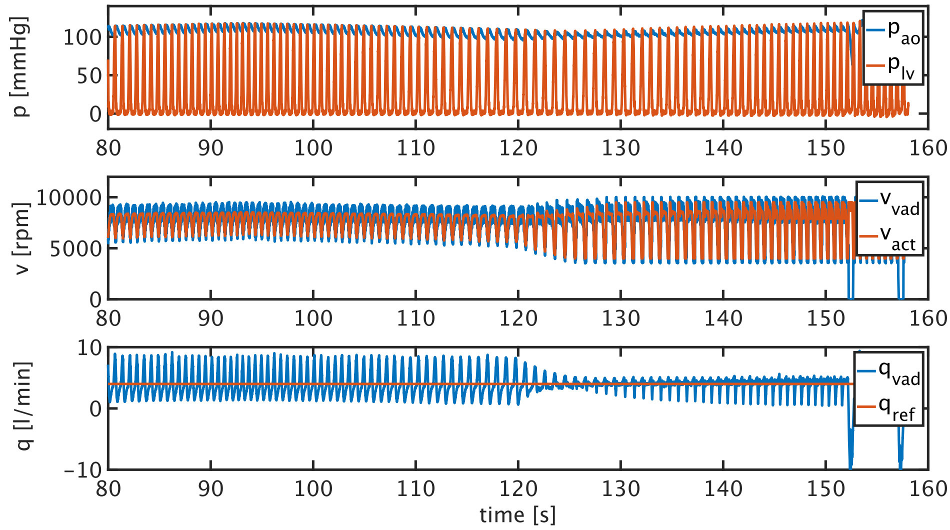

Figure 5.24: Segment of measurement for ILC with varying disturbance with $cf_{\mathrm{Lv}} = 1$ for constant reference flow without data resampling. Top: pressure values of the MCL. Middle: actuating variable and measured rotational speed of the VAD. Bottom: targeted flow trajectory and measured flow through the VAD.

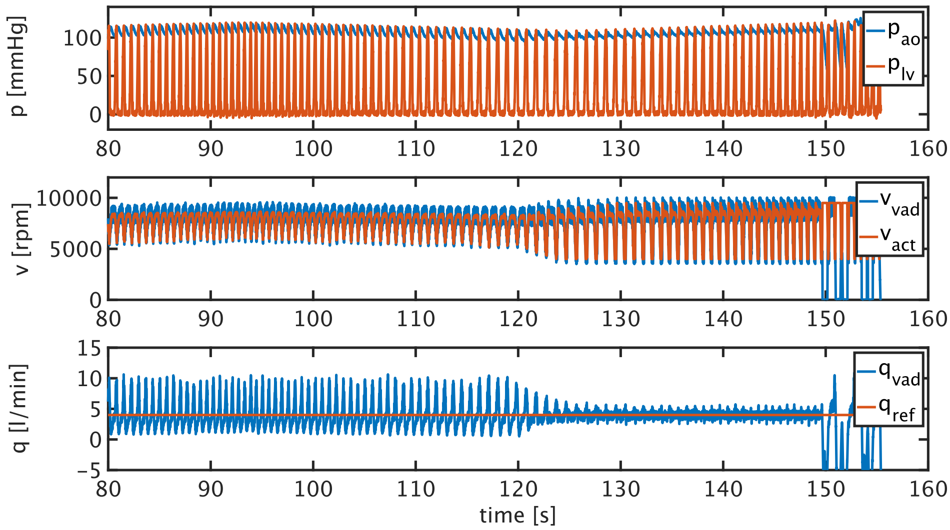

Figure 5.25: Segment of measurement for ILC with varying disturbance with $cf_{\mathrm{Lv}} = 1$ for constant reference flow with data resampling. Top: pressure values of the MCL. Middle: actuating variable and measured rotational speed of the VAD. Bottom: targeted flow trajectory and measured flow through the VAD.

This suggests a higher performance of the ILC using the resampling functionality. This assumption can be confirmed when comparing the RMSE values of the two measurements. While at the beginning of combined control both measurements decrease to an average error value of

$$RMSE_{\text{const,low}} = RMSE_{\text{resampled,const}} \approx 0.05\, l/min \tag{5.31}$$

the value of the measurement without resampling the data afterwards increases continuously to a value of

$$RMSE_{\text{const,high}} \approx 1.13\, l/min. \tag{5.32}$$

The value of the measurement with resampled data remains at about $0.05\, l/min$. Thus, for a constant reference flow, a significant improvement in performance can be achieved by resampling the data of the actuating variable before the output is applied to the plant. Figure 5.26 depicts a graphical comparison of the RMSE courses of the two measurements.

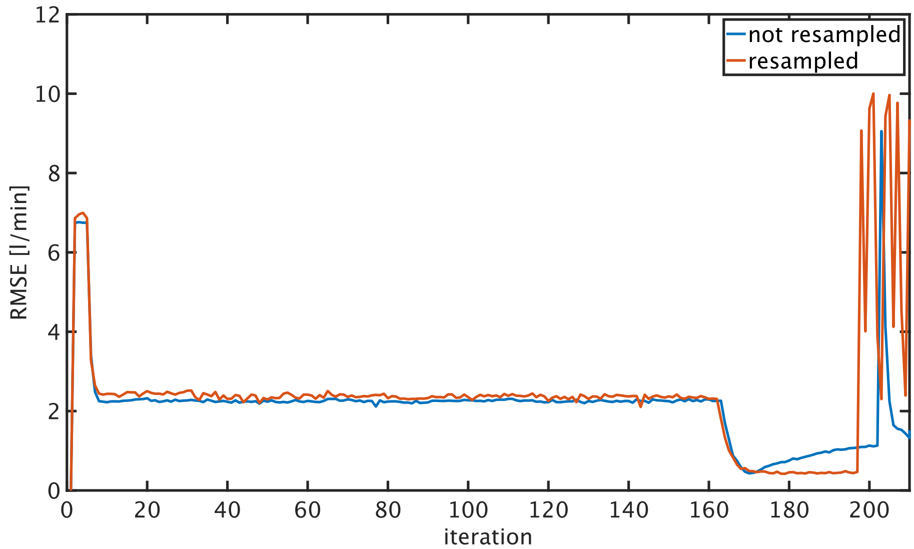

Figure 5.26: Comparison of RMSE values for ILC measurement using a constant reference flow for unchanged and resampled data.

The second set of measurements is performed using the sinusoidal reference signal. Other than for the constant reference flow for which both the unchanged ILC and the resampling measurement result in a pump failure after approximately 155 s, the measurements following a sinusoidal trajectory ran stable over the full measurement time of 600 s. Looking at the graphical comparison of the RMSE values of the two measurements, shown in Figure 5.27, significantly lower error values can be seen for the complete measurement period using the resampling functionality. For this, the RMSE is about

$$RMSE_{\text{resampled,sine}} \approx 0.3\, l/min \tag{5.33}$$

from the onset of the ILC. For the measurement with the standard P-type ILC, permanent fluctuations of the RMSE between

$$RMSE_{\text{sine,low}} \approx 0.3\, l/min \tag{5.34}$$

and

$$RMSE_{\text{sine,high}} \approx 0.9\, l/min \tag{5.35}$$

can be seen. Thus, an increased performance of the revised ILC can also be concluded for this reference trajectory.

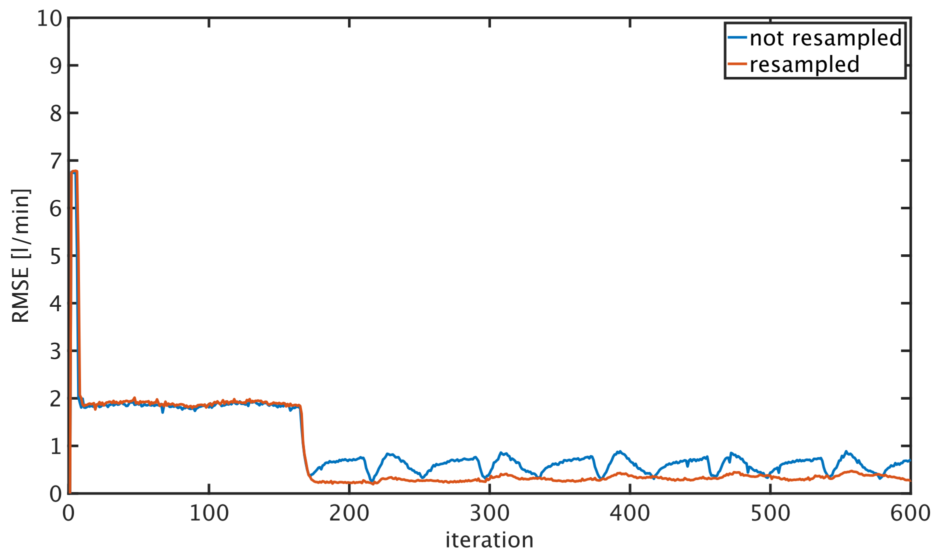

Figure 5.27: Comparison of RMSE values for ILC measurement using a sinusoidal reference flow for unchanged and resampled data.

The measurements using the triangular reference trajectory show very similar system behavior to those using the constant reference flow. Both when using the standard ILC and the revised ILC, the pump stops due to oscillating system behavior. This occurs slightly earlier for the measurement using the revised ILC than for the standard ILC. However, when comparing the RMSE values in Figure 5.28 it is clear that the performance of the revised ILC exceeds that of the unmodified ILC. While the revised ILC has average error values of about

$$RMSE_{\text{resampled,triang}} \approx 0.38\, l/min, \tag{5.36}$$

the value for the standard ILC initially drops to about

$$RMSE_{\text{triang,low}} \approx 0.46\, l/min \tag{5.37}$$

but then rises continuously to a value of

$$RMSE_{\text{triang,high}} \approx 0.79\, l/min. \tag{5.38}$$

Thus, even though the pump stops earlier, the use of the revised ILC would be advisable.

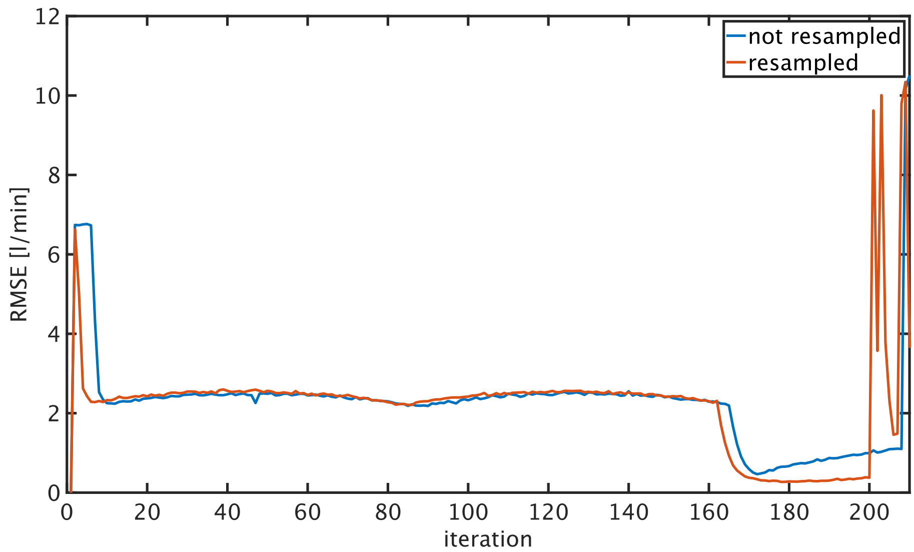

Figure 5.28: Comparison of RMSE values for ILC measurement using a triangular reference flow for unchanged and resampled data.

Lastly, the tests of the two ILC implementations are performed using the rectangular reference trajectory. As with the constant reference flow and the triangular trajectory, the actuating variable again oscillates, resulting in the pump rotor stopping. Unlike the previous measurements, however, the evaluation of the error values for both measurements is similar in this case. At the beginning of the combined control, the averaged error values for both tests drop sharply compared to the PI control. However, a fluctuation of the average error values can be observed for both measurements. This occurs somewhat more slowly for the revised ILC than for the standard ILC. Nevertheless, both measurements show best case values of about

$$RMSE_{\text{resampled,rect,low}} = RMSE_{\text{rect,low}} \approx 0.4\, l/min, \tag{5.39}$$

and worst case values of about

$$RMSE_{\text{resampled,rect,high}} = RMSE_{\text{rect,high}} \approx 0.77\, l/min. \tag{5.40}$$

A graphical comparison is presented in Figure 5.29.

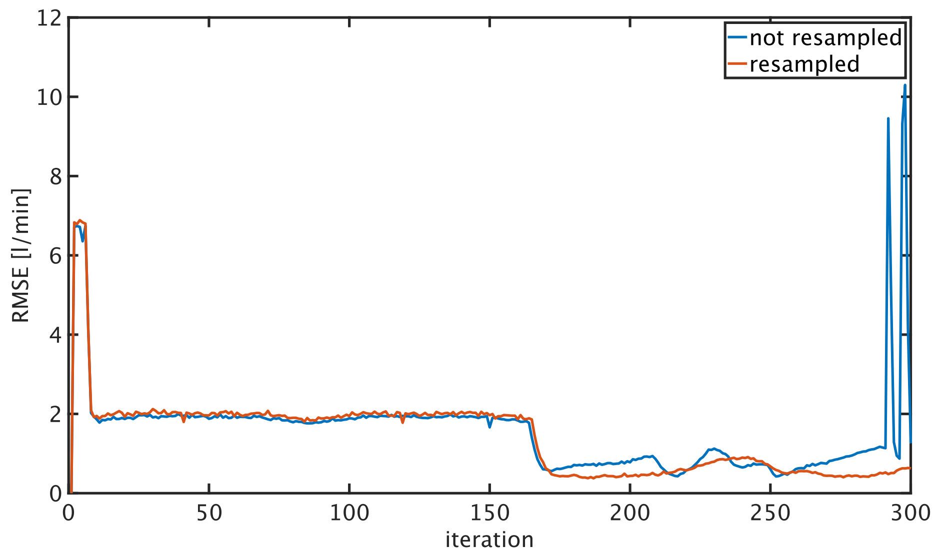

Figure 5.29: Comparison of RMSE values for ILC measurement using a rectangular reference flow for unchanged and resampled data.

These results do not give a clear indication as to which ILC approach is more suitable for reference tracking of this trajectory.

Graphical representations of the transitional segments for the performed measurements using sinusoidal, triangular and rectangular reference trajectories can be found in Figure A.9 to Figure A.14 of the appendix.

Table 5.1 depicts an overview on the worst case RMSE values of the standard ILC and for the revised ILC for all reference trajectories. It furthermore gives the difference between these error values as $\Delta RMSE$.

reference trajectory	$RMSE_{\text{std\_ILC,high}}$ $[l/min]$	$RMSE_{\text{resampled}}$ $[l/min]$	$\Delta RMSE$ $[l/min]$
constant flow	1.13	0.05	1.08
sinusoidal	0.9	0.3	0.6
triangular	0.79	0.38	0.41
rectangular	0.77	0.77	-

Table 5.1: RMSE values for different reference trajectories of standard ILC and revised ILC.

The highest improvement is achieved for the constant reference flow with $\Delta RMSE = 1.08\,l/min$. Also, for constant reference flow, the highest overall performance is achieved with an RMSE of only $0.05\,l/min$. This can be explained by the fact that the length of the reference signal does not change for a constant flow, while this is the case for all other signals.

6 Conclusion and future work

6.1 Conclusion

As the gap between the incidence of cardiovascular disease and the availability of donor organs will continue to grow in the coming years due to demographic change, it is of increasing importance to further develop alternative therapies for CVDs. For this reason, a flow control system for the Sputnik VAD axial flow pump was developed in the context of this work, enabeling the system to follow different predefined flow trajectories.
This was achieved by a stepwise development and optimization of a control loop, which comprises a parallel architecture of a PI controller and an ILC.
First, the performance of two PI controllers, designed using the Ziegler Nichols and Chien Hrones Reswick methods, was compared. The second one showed a significantly higher performance, which led to its further use within the ILC implementation as a stabilizing feedback controller.
After successful optimization of the Q-filter implemented within the ILC, a series of tests were performed to determine the quality of the ILC. Under the idealized assumption of disturbance by a heartbeat with regular heart rate of $60\,bpm$ and adjustment of the length of the flow trajectories to a duration of $1\,s$ per iteration, satisfactory results were obtained with averaged error values ranging from $RMSE_{\text{rect}} = 0.22\,l/min$ for a rectangular trajectory to $RMSE_{\text{sine}} = 0.09\,l/min$ for a sinusoidal trajectory. When the standard ILC was subjected to a non-repetitive disturbance in the form of heartbeats of variable heart rates, a significant degradation in performance was evident. For this case, the averaged error values amounted to $RMSE_{\text{rect}} = 0.77\,l/min$ for the rectangular signal. For a constant reference flow, it peaked at $RMSE_{\text{const}} = 1.13\,l/min$.
In order to ensure high performance even in the presence of variable disturbances, the ILC was extended by further data preprocessing in the form of resampling of the ILC's actuating variable data to an iteration length corresponding to the current heart rate. This allowed the averaged error values for a constant flow to be reduced to just $RMSE_{\text{resampled,const}} = 0.05\,l/min$. A noticeable improvement in performance

was also achieved for a sinusoidal and a triangular signal with RMSE reductions of $\Delta RMSE = 0.6\, l/min$ and $\Delta RMSE = 0.41\, l/min$, respectively. Only for the rectangular signal no clear increase in performance could be seen. For all reference trajectories tested, however, the pump stopped after some time because the actuating variable exhibited oscillating behavior.

6.2 Future work

In order to ensure long-term flow control under the influence of non-repeating disturbances, as would be necessary for use on patients, the robustness of the controller to this type of disturbance would have to be optimized.
Conceivable approaches to achieve this goal could be given in the use of other ILC implementations, such as a current iteration learning control. Also, the use of a higher-order learning algorithm, which uses not only the last but also even earlier iterations for the calculation, would be recommendable.
Since the rotor of the pump stopped for all tested reference trajectories of the revised ILC, it would be advisable to use an alternative control unit in order to improve robustness of the control system. One possible hardware change would be to use the original control unit associated with the Sputnik VAD instead of the ESCON 50/4 EC-S.
For employment of the resampling functionality, as implemented in this work to improve the ILC for non-repetitive disorders, the additional analysis of ECG data to gain information on the heart rate would be necessary in clinical use. However, since the Sputnik VAD is a therapeutic option with the therapeutic goal of bridging to transplantation, it is conceivable that a patient may require prolonged support from the system. In such a case, it would be desirable not to restrict the patient's mobility and quality of life with an additional medical device. For this reason, a further development of the ILC approach, which would make the use of an ECG signal obsolete, would be desirable. Possible approaches to this could be through analysis of the motor current of the pump or by including a flow estimation approach. Furthermore, extending the pump with a pressure sensor and determining the heart beat from pressure changes would be conceivable.

A Appendix

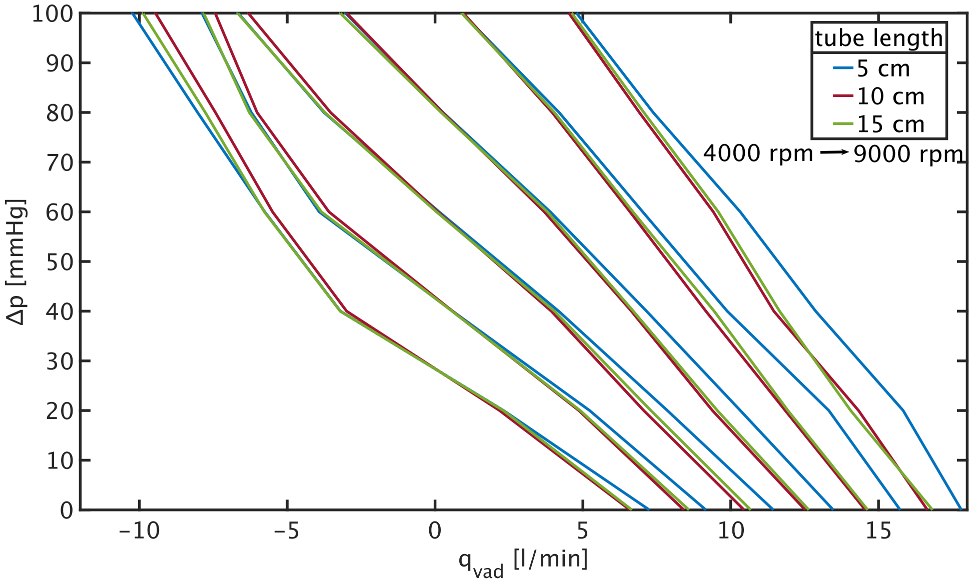

Figure A.1: Static map for varying tube length in 100 % water.

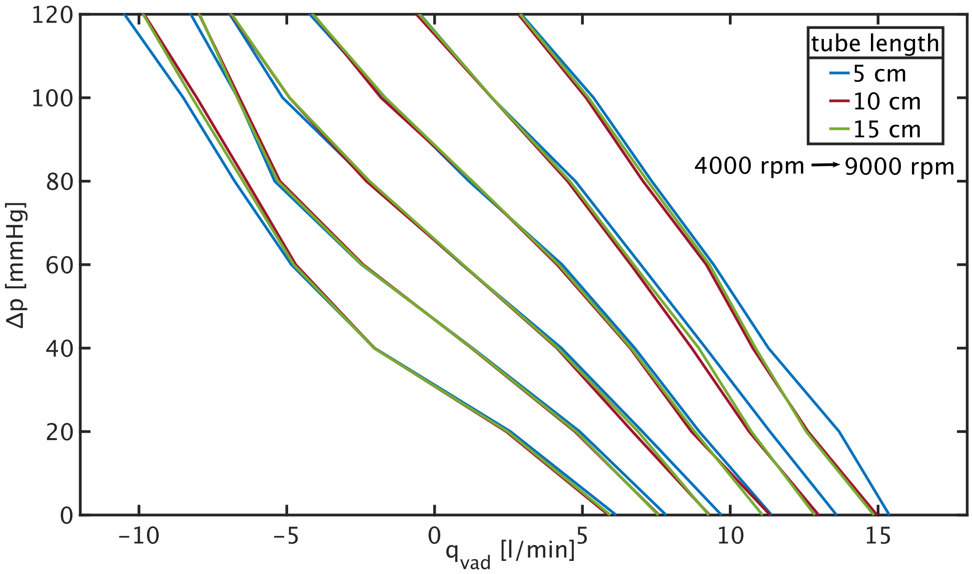

Figure A.2: Static map for varying tube length in 80 % water 20 % glycerin solution.

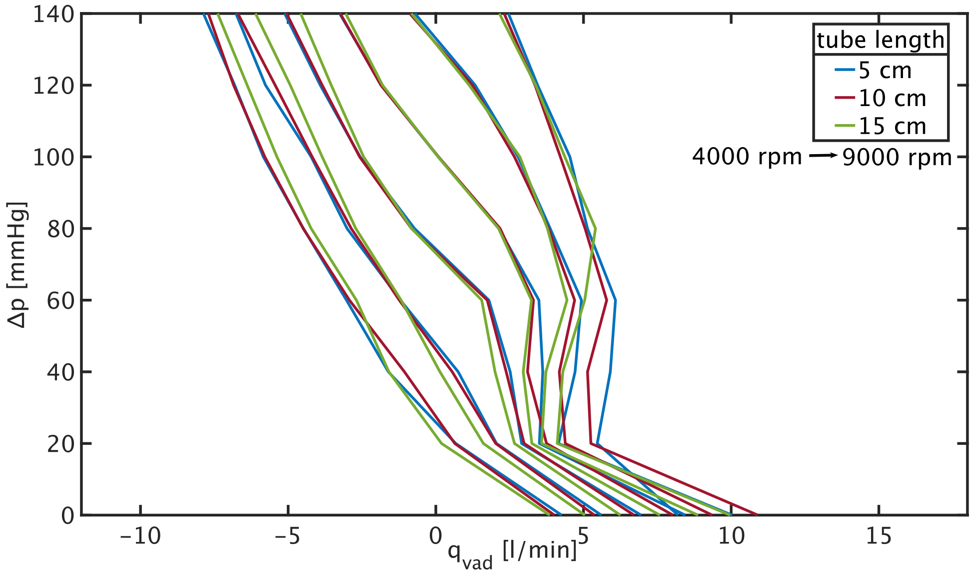

Figure A.3: Static map for varying tube length in 40 % water 60 % glycerin solution.

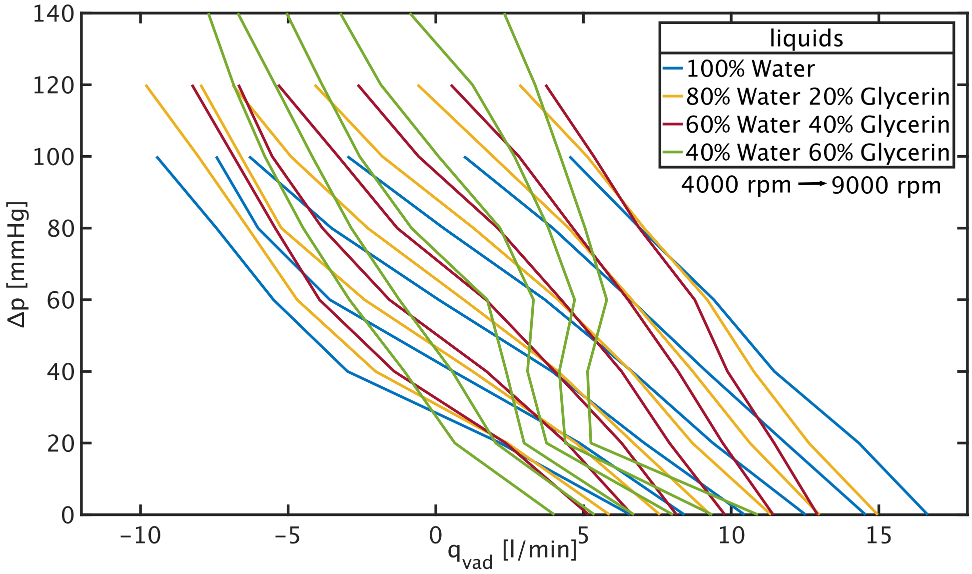

Figure A.4: Static map for varying liquid solutions with 10 cm tube length.

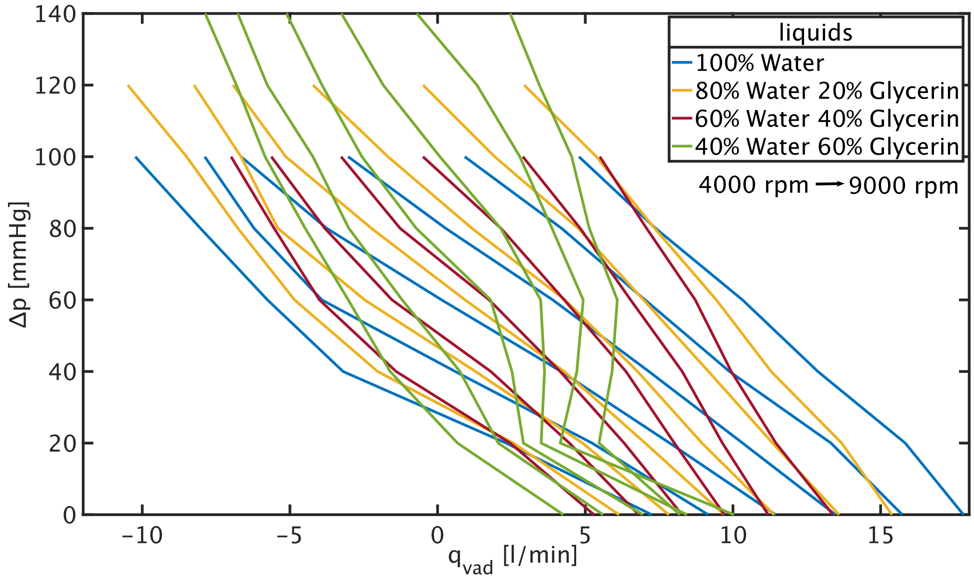

Figure A.5: Static map for varying liquid solutions with 5 cm tube length.

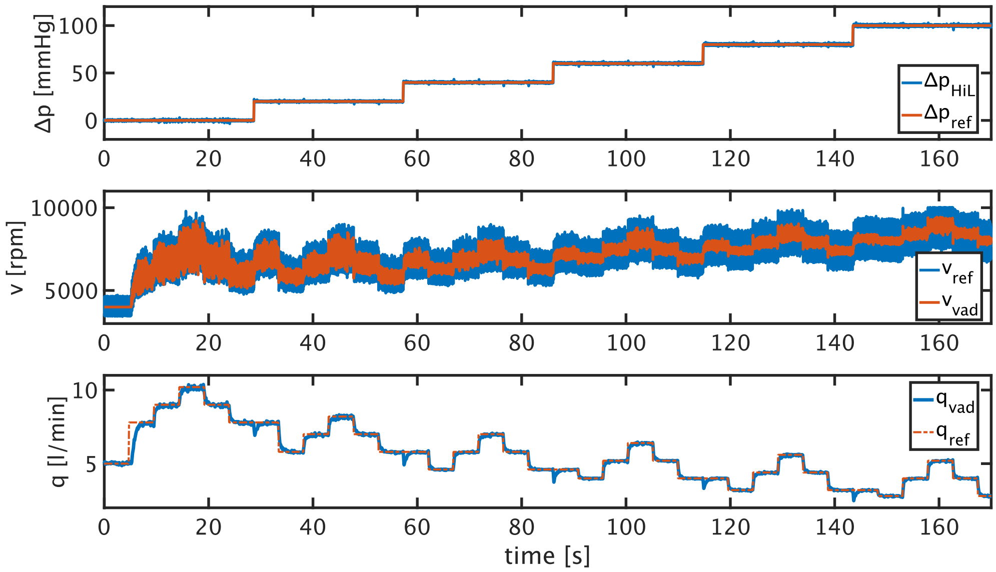

Figure A.6: Test measurement for PI controller tuned according to Chien Hrones Reswick.

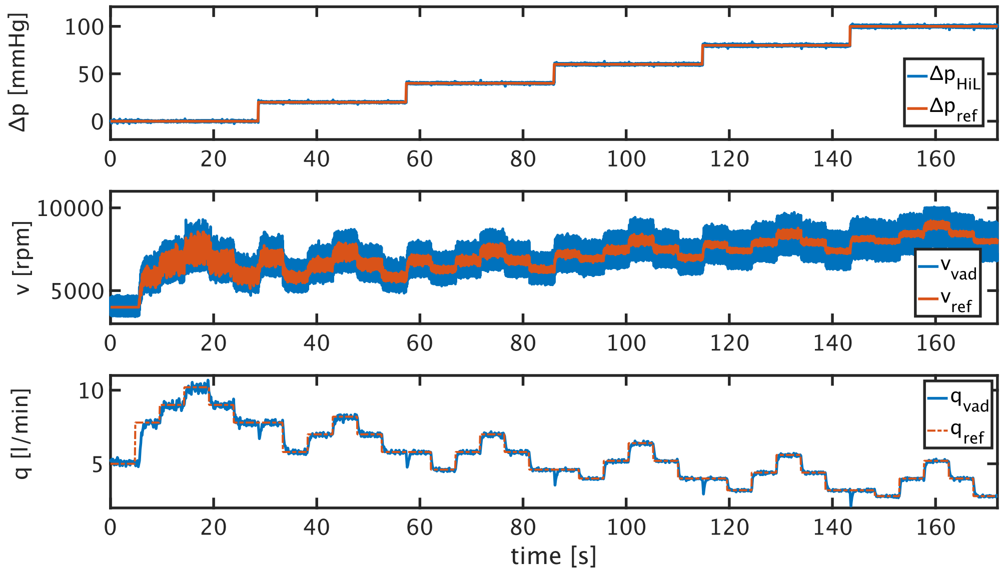

Figure A.7: Test measurement for PI controller tuned according to Ziegler Nichols.

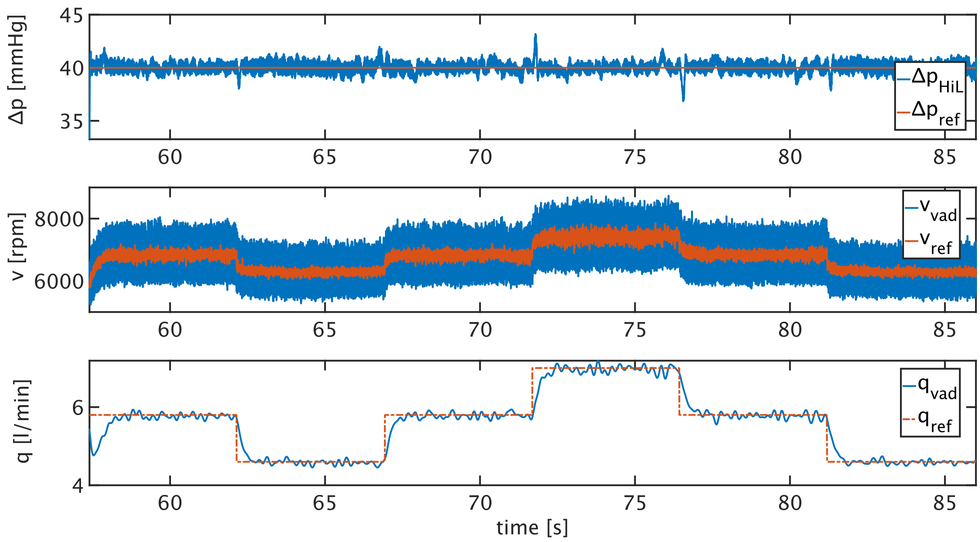

Figure A.8: Test measurement for PI controller tuned according to Ziegler Nichols at $\Delta p = 40\,mmHg$.

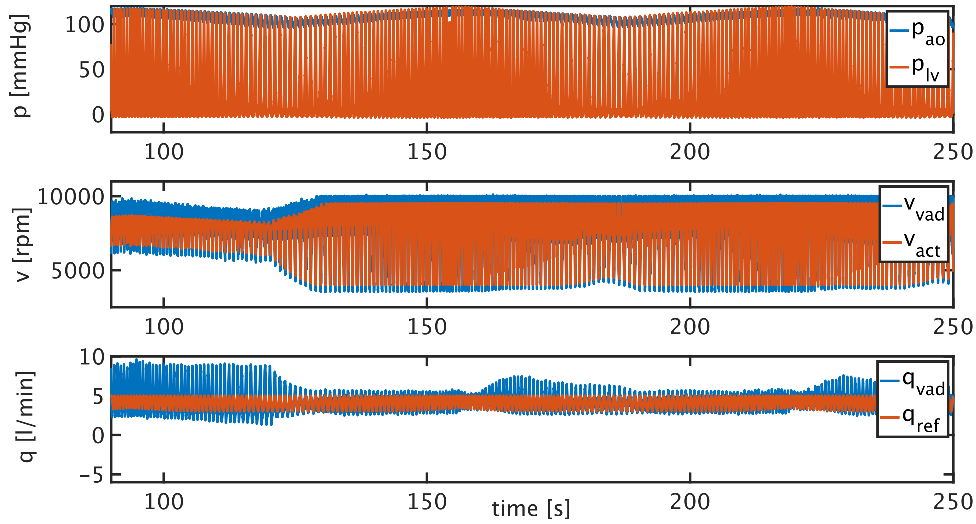

Figure A.9: Segment of measurement for ILC with varying disturbance with $cf_{\mathrm{Lv}} = 1$ for sinusoidal reference flow without data resampling. Top: pressure values of the MCL. Middle: actuating variable and measured rotational speed of the VAD. Bottom: targeted flow trajectory and measured flow through the VAD.

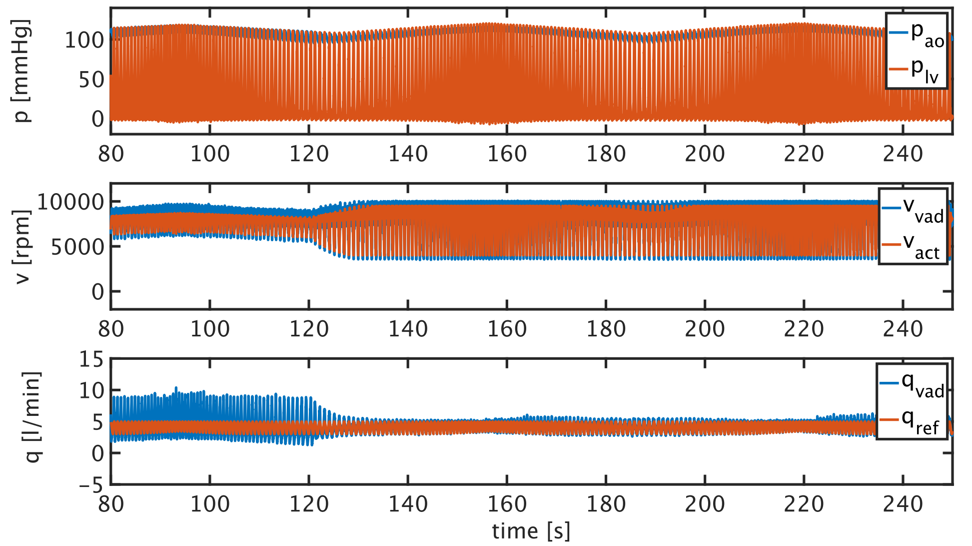

Figure A.10: Segment of measurement for ILC with varying disturbance with $cf_{\mathrm{Lv}} = 1$ for sinusoidal reference flow with data resampling. Top: pressure values of the MCL. Middle: actuating variable and measured rotational speed of the VAD. Bottom: targeted flow trajectory and measured flow through the VAD.

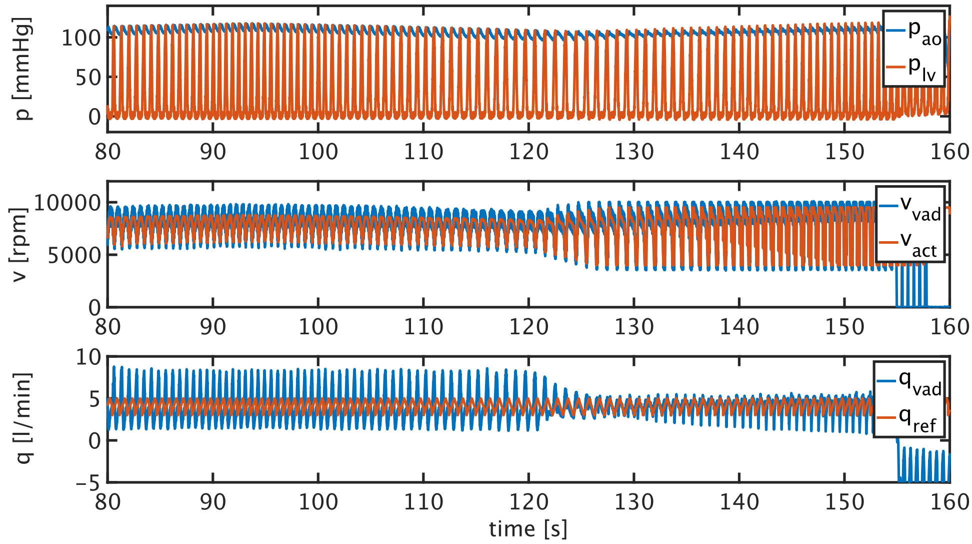

Figure A.11: Segment of measurement for ILC with varying disturbance with $cf_{\mathrm{Lv}} = 1$ for triangular reference flow without data resampling. Top: pressure values of the MCL. Middle: actuating variable and measured rotational speed of the VAD. Bottom: targeted flow trajectory and measured flow through the VAD.

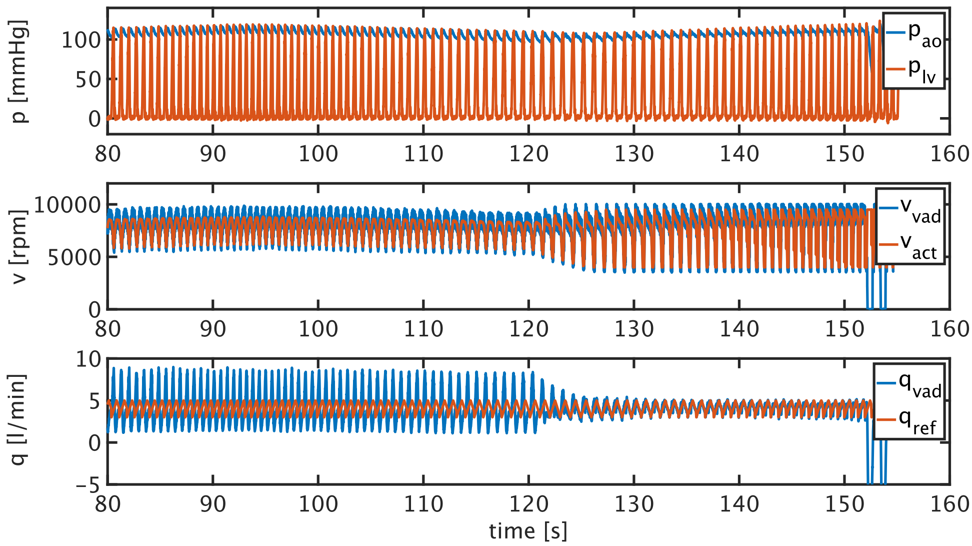

Figure A.12: Segment of measurement for ILC with varying disturbance with $cf_{\mathrm{Lv}} = 1$ for triangular reference flow with data resampling. Top: pressure values of the MCL. Middle: actuating variable and measured rotational speed of the VAD. Bottom: targeted flow trajectory and measured flow through the VAD.

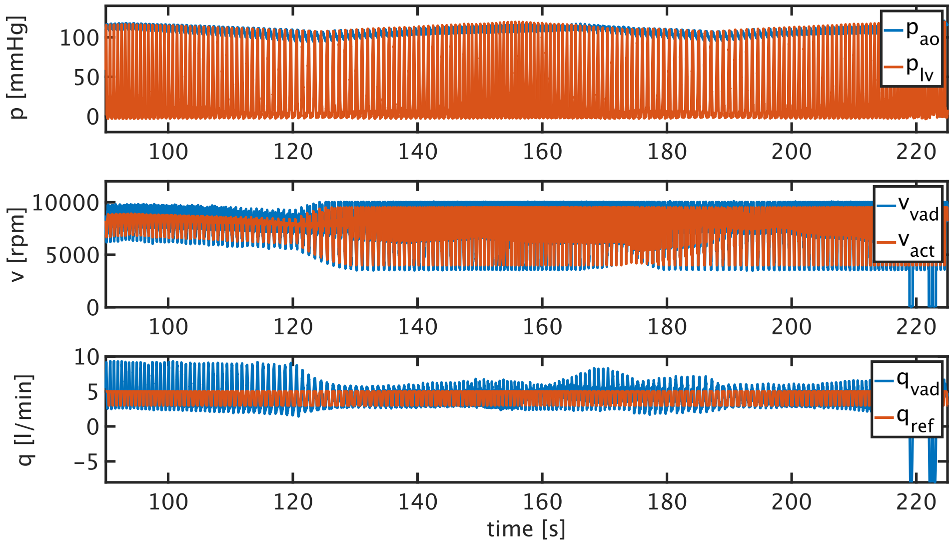

Figure A.13: Segment of measurement for ILC with varying disturbance with $cf_{\mathrm{Lv}} = 1$ for rectangular reference flow without data resampling. Top: pressure values of the MCL. Middle: actuating variable and measured rotational speed of the VAD. Bottom: targeted flow trajectory and measured flow through the VAD.

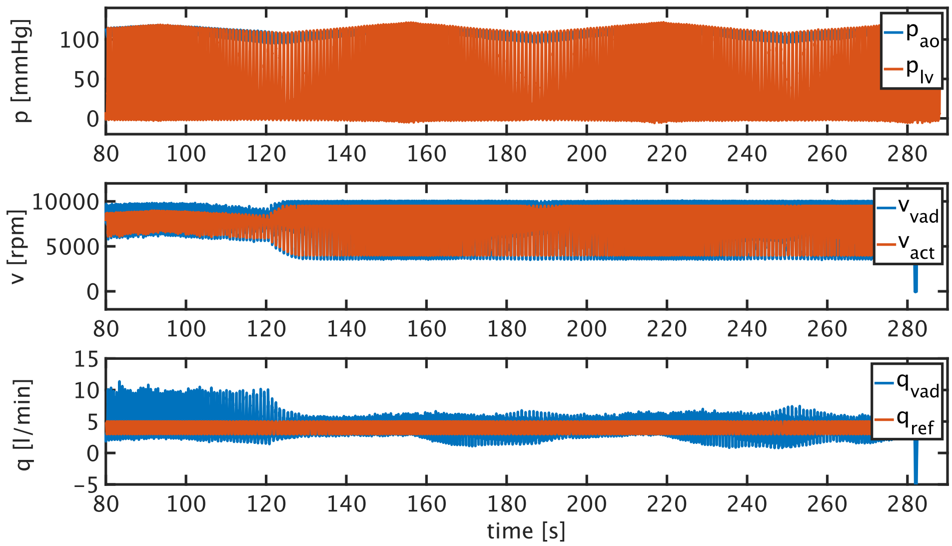

Figure A.14: Segment of measurement for ILC with varying disturbance with $cf_{\mathrm{Lv}} = 1$ for rectangular reference flow with data resampling. Top: pressure values of the MCL. Middle: actuating variable and measured rotational speed of the VAD. Bottom: targeted flow trajectory and measured flow through the VAD.

Bibliography

[AHR11] ARORA, Ashish ; HOTE, Yogesh V. ; RASTOGI, Mahima: Design of PID Controller for Unstable System. In: BALASUBRAMANIAM, P. (Hrsg.): *Control, Computation and Information Systems*. Berlin, Heidelberg : Springer Berlin Heidelberg, 2011. – ISBN 978–3–642–19263–0, S. 19–26

[BTA06] BRISTOW, D.A. ; THARAYIL, M ; ALLEYNE, A.G.: A survey of iterative learning. In: *Control Systems, IEEE* 26 (2006), 07, S. 96 – 114. http://dx.doi.org/10.1109/MCS.2006.1636313. – DOI 10.1109/MCS.2006.1636313

[CD14] CHAI, T. ; DRAXLER, R. R.: Root mean square error (RMSE) or mean absolute error (MAE)? In: *Geoscientific Model Development Discussions* 7 (2014), Februar, Nr. 1, S. 1525–1534. http://dx.doi.org/10.5194/gmdd-7-1525-2014. – DOI 10.5194/gmdd–7–1525–2014

[DMH19] DASHKEVICH, A ; MICHEL, S ; HAGL, C: Indikationsstellung und Therapieziele der mechanischen Kreislaufunterstützung. In: *Medizinische Klinik-Intensivmedizin und Notfallmedizin* 114 (2019), Nr. 5, S. 452–458

[Eif18] EIFERT, S: Perkutane und chirurgische Optionen der mechanischen Kreislaufunterstützung in der Therapie der terminalen Herzinsuffizienz. In: *Der Anaesthesist* 67 (2018), Nr. 5, S. 321–325

[GSL+03] GRABELLUS, F. ; SCHMID, C. ; LEVKAU, B. ; STYPMANN, J. ; SCHELD, H. ; BABA, Hideo A.: Myokardiale Veränderungen unter mechanischer linksventrikulärer Unterstützungstherapie. In: *Der Pathologe* 24 (2003), Nr. 2, S. 83–90

[Hal16] HALL, John E.: *Guyton and Hall Textbook of Medical Physiology, Jordanian Edition E-Book*. Elsevier, 2016

[KPK+17] KIRKLIN, James K. ; PAGANI, Francis D. ; KORMOS, Robert L. ; STEVENson, Lynne W. ; Blume, Elizabeth D. ; Myers, Susan L. ; Miller, Marissa A. ; Baldwin, J. T. ; Young, James B. ; Naftel, David C.: Eighth annual INTERMACS report: Special focus on framing the impact of adverse events. In: *The Journal of Heart and Lung Transplantation* 36 (2017), 2020/08/05, Nr. 10, S. 1080–1086

[KR15] Katz, Arnold M. ; Rolett, Ellis L.: Heart failure: when form fails to follow function. In: *European Heart Journal* 37 (2015), 10, Nr. 5, 449-454. `http://dx.doi.org/10.1093/eurheartj/ehv548`. – DOI 10.1093/eurheartj/ehv548. – ISSN 0195–668X

[KSS+11] Krabatsch, T ; Schweiger, M ; Stepanenko, A ; Drews, T ; Potapov, E ; Pasic, M ; Weng, Y ; Huebler, M ; Hetzer, R: Fortschritte bei implantierbaren mechanischen Kreislaufunterstüzungssystemen. In: *Herz* 36 (2011), Nr. 7, S. 622

[LHH+63] Liotta, Domingo ; Hall, C.William ; Henly, Walter S. ; Cooley, Denton A. ; Crawford, E.Stanley ; DeBakey, Michael E.: Prolonged assisted circulation during and after cardiac or aortic surgery: Prolonged partial left ventricular bypass by means of intracorporeal circulation. In: *The American Journal of Cardiology* 12 (1963), Nr. 3, S. 399 – 405. – ISSN 0002–9149. – Symposium on Cardiovascular-Pulmonary Problems Before and After Surgery Part I

[Lun10] Lunze, Jan: *Regelungstechnik 1: Systemtheoretische Grundlagen, Analyse und Entwurf einschleifiger Regelungen.* Berlin, Heidelberg : Springer Berlin Heidelberg, 2010. `http://dx.doi.org/10.1007/978-3-642-13808-9_1`. `http://dx.doi.org/10.1007/978-3-642-13808-9_1`. – ISBN 978–3–642–13808–9

[LW16] *Kapitel* Herzunterstützungssysteme. In: Leonhardt, Steffen ; Walter, Marian: *Medizintechnische Systeme: Physiologische Grundlagen, Gerätetechnik und automatisierte Therapieführung.* Berlin, Heidelberg : Springer Berlin Heidelberg, 2016. – ISBN 978–3–642–41239–4, S. 107–144

[MRS+15] Misgeld, Berno J. ; Rüschen, Daniel ; Schwandtner, Sebastian ; Heinke, Stefanie ; Walter, Marian ; Leonhardt, Steffen: Robust decentralised control of a hydrodynamic human circulatory system simulator. In: *Biomedical Signal Processing and Control* 20 (2015), 35 - 44. `http://dx.doi.org/https://doi.org/10.1016/j.bspc.2015.04.004`. – DOI https://doi.org/10.1016/j.bspc.2015.04.004. – ISSN 1746–8094

[MS09] Meyer, Anna L. ; Strüber, Martin: Chronische Therapie durch linksventrikuläre Unterstützungssysteme bei terminaler Herzinsuffizienz. In: *Herz Kardiovaskuläre Erkrankungen* 34 (2009), Nr. 2, S. 148–153

[SBL19] Sponga, Sandro ; Benedetti, Giovanni ; Livi, Ugolino: Short-term mechanical circulatory support as bridge to heart transplantation: paracorporeal ventricular assist device as alternative to extracorporeal life support. In: *Annals of cardiothoracic surgery* 8 (2019), 01, Nr. 1, S. 143–150

[Sch10] Schüller, Annika: Das Kunstherz – Möglichkeiten der mechanischen Kreislaufunterstützung (VAD). In: *intensiv* 18 (2010), Nr. 03, S. 138–147

[SH19] Shehab, Sajad ; Hayward, Christopher S.: Choosing Between Left Ventricular Assist Devices and Biventricular Assist Devices. In: *Cardiac failure review* 5 (2019), 02, Nr. 1, S. 19–23

[SK07] Schiebler, Theodor H. ; Korf, Horst-W: *Anatomie: Histologie, Entwicklungsgeschichte, makroskopische und mikroskopische Anatomie, Topographie*. Springer-Verlag, 2007

[SLH11] Schmidt, Robert F. ; Lang, Florian ; Heckmann, Manfred: *Physiologie des Menschen mit Pathophysiologie*. Springer-Verlag, 2011

[ST15] Selishchev, Sergey ; Telyshev, Dmitry: Ventricular assist device Sputnik: Description, technical features and characteristics. In: *Trends in Biomaterials and Artificial Organs* 29 (2015), Nr. 3, S. 207–210

[ST16] SELISHCHEV, Sergey ; TELYSHEV, Dmitry: Optimisation of the Sputnik-VAD design. In: *The International journal of artificial organs* 39 (2016), 09. http://dx.doi.org/10.5301/ijao.5000518. – DOI 10.5301/ijao.5000518

[Wor20] WORLD HEALTH ORGANIZATION: *Cardiovascular diseases (CVDs)*. https://www.who.int/news-room/fact-sheets/detail/cardiovascular-diseases-(cvds), Zuletzt besucht am 06.08.2020

[ZR17] ZACHER, Serge ; REUTER, Manfred: *Regelungstechnik für Ingenieure: Analyse, Simulation und Entwurf von Regelkreisen*. Wiesbaden : Springer Fachmedien Wiesbaden, 2017. http://dx.doi.org/10.1007/978-3-658-17632-7_3. http://dx.doi.org/10.1007/978-3-658-17632-7_3. – ISBN 978–3–658–17632–7